Advances in Nano Research, *Vol. 11, No. 2 (2021) 115-140*
https://doi.org/10.12989/anr.2021.11.2.115

Vibration characteristics of microplates with GNPs-reinforced epoxy core bonded to piezoelectric-reinforced CNTs patches

Masoud Forsat[1], Farayi Musharavati[1], Elsadig Eltai[1], Azlan Mohd Zain[2], Saleh Mobayen*[3] and Abdeliazim Mustafa Mohamed[4],

[1]*Department of Mechanical and Industrial Engineering Qatar University, P.O. Box 2713, Doha, Qatar*
[2]*UTM Big Data Centre, Universiti Teknologi Malaysia 81310 Johor, Malaysia*
[3]*Future Technology Research Center, National Yunlin University of Science and Technology, 123 University Road, Section 3, Douliou, Yunlin 64002, Taiwan, R.O.C.*
[4]*Department of Civil Engineering, College of Engineering, Prince Sattam bin Abdulaziz University, Alkharj 16273, Saudi Arabia*

(*Received September 11, 2020, Revised November 30, 2020, Accepted December 3, 2020*)

Abstract. In the current study, vibration characteristics of a three-layered rectangular microplate with Graphene nanoplatelets (GNPs)-reinforced Epoxy core which is fully bonded to piezoelectric-reinforced single-walled Carbon nanotubes (SWCNTs) patches are provided. The face sheets are subjected to the electric field and the microplate is assumed to be in a thermal environment and also, is located on the visco-Pasternak model of the elastic substrate. The GNPs and SWCNTs are dispersed through the core's and face's thickness according to the given functions. To account the shear deformation effect, tangential shear deformation theory (TGSDT) as a higher-order theory is employed and the modified strain gradient theory (MSGT) with tree independent length-scale parameters is selected to capture the size effect. Using the extended form of Hamilton's principle and variational formulation, the governing motion equations are derived and solved mathematically via Navier's scheme for simply supported edges microplate. By ensuring the validity of the results after comparing them in a simpler state with previously published ones, the effects of the most prominent parameters on the results are investigated. It is seen GNPs and CNTs dispersion patterns play an important role in the microplate vibrational behavior, as well as temperature variations. Since the under consideration microstructure can be accounted as smart structures, therefore, the outcomes of this study may help to design and create more efficient engineering structures, such as sensors and actuators and also micro/nano electromechanical systems.

Keywords: carbon nanotubes; graphene nanoplatelets; modified strain gradient theory; sandwich structures; thermal environment; vibration analysis

1. Introduction

Regarding the rapid growth of material science, the researchers have focused on new materials and investigate their influence on the mechanical properties of engineering structures. To improve the properties of structures, reinforced composites have found extensive applications these days. Carbon nanotubes (CNTs) and graphene nanoplatelets (GNPs) are the two most well-known nano reinforcements due to their unique specifications. Iijima (1991) discovered CNTs in the 1990s. After that, studies have shown that due to its high elastic modulus, it can be a useful and valuable component in engineering structures. Vibration analysis of a CNTs-reinforced composite plate was performed via the finite element method based on the first-order shear deformation theory (FSDT) by Zhu *et al.* (2012). They considered different types of CNTs distributions and boundary conditions. Stability analysis of three-phase sandwich laminated nanocomposite panels which were nonlinearly imperfect was presented by Van Thu and Duc (2016). Loghman and Cheraghbak (2018) considered agglomeration effects on the behavior of nanocomposite piezoelectric cylinders. They assumed that the structure was under internal pressure and CNTs selected as the reinforcement of the composite. Mirzaei and Kiani (2016) used the refined mixture rule to analyze cylindrical panels made from functionally graded (FG)-CNTs reinforced composites. They considered different effects of CNTs on the results. Applying the Ritz method, Selim *et al.* (2016) obtained the natural frequencies of FG-CNTs reinforced composites plates. They accounted for thermal effects on the results and investigated both uniform and FG distributions of CNTs and studied the effect of different parameters on the results. The dynamic response of piezoelectric FG sandwich cylindrical shells was investigated by Duc (2018) considering the shear deformation effect. Also, Mehar *et al.* (2017) used the finite element method (FEM) to solve the nonlinear equations of a doubly curved FG-CNTs reinforced composites shell. The structure was in a thermal environment and was modeled based on higher-order shear deformation theory and Green-Lagrange strains. Static bending analysis of FG polymer

*Corresponding author, Ph.D.,
E-mail: mobayens@yuntech.edu.tw

Copyright © 2021 Techno-Press, Ltd.

ISSN: 2287-237X (Print), 2287-2388 (Online)

composite curved beams reinforced with CNTs considered by Talebizadehsardari *et al*. (2020). A comprehensive analytical study on FG-CNTs reinforced composite plates conducted by Karami *et al*. (2018). The size-dependent characteristics of elastic guided waves in an FG-CNTs reinforced composite plate with fully clamped ends conducted by Karami *et al*. (2019d). Nonlinear forced vibrations of multi-scale epoxy/CNT/fiberglass truncated conical shells and annular plates considered by Mirjavadi *et al*. (2020b). Also, they (Mirjavadi *et al*. 2020a) presented another study about a multi-scale epoxy/CNT/fiberglass annular sector plate in the view of determining nonlinear forced vibration characteristics. GNPs were also studied by Novoselov *et al*. (2004) who is known as the first researcher discovering their extreme properties. Most recently, the researchers are attracted to GNPs due to their excellent properties such as high stiffness to mass ratio and high thermal conductivity which introduced the GNPs as reinforcements outperforming CNTs. It is noteworthy that GNPs weight fraction and dispersion patterns are the most effective factors in the mechanical properties of GNP-reinforced composites. Due to lightweight and high stiffness, the functionally graded-graphene nanoplatelets (FG-GNPs) reinforced composites have found a wide range of applications. Behdinan *et al*. (2020) discussed GNPs and CNTs' impact on the heat transfer response of nanocomposite cylinders. García-Macías *et al*. (2018) compared the effect of the GNPs vs. CNTs on the free vibration behavior of reinforced composite plates. They also included the agglomeration effect of the nanocomposite. Their findings showed an extreme load-bearing capacity of GNPs reinforced composite plates. Liu *et al*. (2020) considered the effect of GNPs reinforcement on the nonlinear resonance of FG beams. Their consideration was based on the Euler-Bernoulli beams theory and they assumed that the GNPs were dispersed through the thickness of the beam based on four different patterns and investigated its effect on the results. Karami and Shahsavari (2020) explored the forced resonant vibration of an FG doubly-curved shell which was reinforced by GNPs. They employed Halpin-Tsai (H-T) and the rule of mixture (RM) to determine the effective properties of the reinforced composites. They also derived the governing equations based on the third-order shear deformation theory (TSDT) which were solved by Navier's series. The dynamics of GNPs reinforced composites shell under a moving harmonic load were studied by Eyvazian *et al*. (2020). They used FSDT as the displacement field and investigated the results based on variations in the most important parameters. Habibi *et al*. (2019) employed the generalized differential quadrature (GDQ) method to solve the differential equations related to a GNPs reinforced nanoshell which was actuated by piezoelectric layers and obtained the natural frequencies and the critical voltage of the aforementioned structure. Resonance behavior of FG polymer composite nanoplates reinforced with GNPs investigated by Karami *et al*. (2019f). Also, Karami *et al*. (2020) conducted a study about elastic wave characteristics of GNPs reinforced composite nanoplates. An inhomogeneous beam model incorporating size effects was formulated by Sahmani *et al*. (2019) within the framework of a TSDT to analyze the size dependency in vibration behavior of post-buckled laminated FG small-scaled beams made from GNPs-reinforced composite.

In recent years, studies on the beams, shells, and plates are developing and researchers are trying to use new methods to improve or control their behaviors. Using a sandwich structure is one of the best approaches to achieve this goal. A softer core in comparison to stiffer face sheets is one of the most important features of the sandwich structures. So, choosing the appropriate material for core and face sheets are of crucial importance in achieving the best results. Piezoelectric (PE) materials are the appropriate candidates to control and improve the performance of the structure. Ferreira *et al*. (2008) used the GDQ method to obtain the frequencies of a sandwich plate. Shingare and Kundalwal (2019) also studied the electromechanical response of GNPs reinforced composites plates using classical plates theory, Navier's approach, and piezoelectricity theory considering the flexoelectric effects. The results indicated the key role of flexoelectricity in the static and dynamic responses of the plates. Sobhy (2018) analyzed the bending treatment of a doubly-curved nanoshell made of FG-GNPs-reinforced composite which was surrounded by piezoelectromagnetic layers. They assumed the shell is exposed to the thermal load, external electric voltage, and magnetic potential. Analyzing exact nonlinear forced vibrations of two-phase magneto-electro-elastic nanobeams under an elliptic-type force conducted by Mirjavadi *et al*. (2020c). FG multilayer GNPs-reinforced composite plates embedded in piezoelectric layers were considered by Lin *et al*. (2018). They investigated the mentioned structure in terms of buckling, vibration, and aeroelastic analyses. They used the Galerkin method to extract the results which showed that a small amount of GNPs even has a significant effect on the results. In another study, buckling and post-buckling features of a GNPs-reinforced piezoelectric plate were analyzed by Mao and Zhang (2019). They investigated the structure's response under both uniaxial and biaxial loading conditions. Safaei (2020) investigated the effect of embedding a porous core on the free vibration behavior of laminated composite plates. He used FSDT to extract the governing equations and solved them via FEM. A novel four-unknown integral model was used for buckling response of FG sandwich plates resting on elastic foundations under various boundary conditions using Galerkin's approach by Chikr *et al*. (2020). Also, Refrafi *et al*. (2020) presented their study about the effects of hygro-thermo-mechanical conditions on the buckling of FG sandwich plates resting on elastic foundations.

Reinforced composites and piezoelectric materials are also used in sandwich structures as core or face sheet. Abazid (2019) considered the size effect based on the nonlocal strain gradient theory for a piezoelectromagnetic nanoplate. FSDT was used by Amir *et al*. (2018) to study the buckling behavior of the nanocomposite sandwich plate via analytical methods regarding the flexoelectricity effect. The formulation of an annular sector plate with piezoelectric layers was derived by Mohammadzadeh-

Keleshteri *et al*. (2017) regarding large-amplitude deformation, using FSDT and von-Karman assumption for strain-displacement relations; GDQ method was employed to solve the equations.

Due to the difference in results of the macro and micro-scales analyses, the researchers have been interested in studying the small-scale behavior of the structures. Eringen (1983, 2002) was one of the first researchers who explored the small (especially nano-scaled) structures developing his nonlocal theory. Later, studies on small-scale effects have been rapidly expanded and other researchers also found out new hints. For instance, Safaei *et al*. (2019) considered the effect of size on the axial buckling behavior of single-layered graphene sheets embedded in elastic media. In another study, nonlocal elasticity and Reddy plate's theory were used to analyze the vibration response of FG nanoplates rested on two parameters elastic medium by Fattahi *et al*. (2019a). Fattahi *et al*. (2019b) presented a similar study but about buckling behavior that was about nanoplates in which Eringen's non-local elasticity equations were incorporated into FSDT, higher-order shear deformation, and classical plate theories. Matouk *et al*. (2020) used a novel integral Timoshenko beam theory to consider the free vibrational behavior of the FG nanobeams integrated in the hygro-thermal environment. They captured the size effects based on Eringen's nonlocal theory. The buckling behavior of FG nanoplates made of anisotropic material (beryllium crystal as a hexagonal material) was investigated by Karami *et al*. (2019a). Also, in another study, Karami *et al*. (2019c) considered wave propagation of FG anisotropic nanoplates resting on Winkler-Pasternak foundation. Magnetic affected wave characteristics of nanosize plates made of anisotropic material were investigated via the three-dimensional bi-Helmholtz nonlocal strain gradient theory by Karami *et al*. (2019b). Amir *et al*. (2020a) analyzed the vibration of a rectangular porous sandwich nanoplate based on sinusoidal shear deformation (SSDT) and nonlocal theories. They solved the equations using Navier's solution method and discussed the influence of different parameters on the results. Due to the shortcomings of nonlocal theory, the researchers attempted to develop other small-scaled theories (Allahkarami and Nikkhah-Bahrami 2018, Li *et al*. 2019, 2020, Amir *et al*. 2019a, b). Modified couple stress (MCS) and modified strain gradient (MSG) theories are two distinct theories in this micro-scale field. Kolahdouzan *et al*. (2018) analyzed the FG-CNTs reinforced composite sandwich microplate using MCST. Their work was focused on the buckling and vibration responses of the plate. Size-dependent behaviors of thick FG microbeams were investigated by Yu *et al*. (2019). To capture the size effects, they employed an extension of the quasi-3D theory to be integrated with the MCST. The influence of various homogenization models was studied on the free vibration behavior of an FGM curved microbeam which was modeled using the MSGT of elasticity as well as the FSDT investigated by Karami *et al*. (2019e). Buckling and free vibration behaviors of FG microplates were assessed by Mirsalehi *et al*. (2017). They employed the MSGT which suggested three-length scale parameters to capture the size effect on the results and obtained the critical buckling load and natural frequencies of the under consideration structure. Employing the MSGT for size-dependent analysis, Arefi *et al*. (2019) evaluated the thermo-mechanical buckling behavior of a rectangular microplate made from FG-GNPs. Moreover, Arshid *et al*. (2020a) presented a comprehensive study on bending, buckling, and free vibration of an FG-GNPs-reinforced metal foam annular plate. They took the size-dependency into account using both MCS and MSG theories and compared their results with those of classical elasticity theory (CET). MCST was applied by Safarpour *et al*. (2019) to evaluate thermal buckling and free and forced vibrations of a cylindrical shell composed of FG-GNPs. Also, the structure was assumed to be rested on an elastic foundation and its properties were considered temperature-dependent. Axial post-buckling analysis of multilayer FG composite nanoplates reinforced with GNPs based on nonlocal strain gradient theory presented by Sahmani and Aghdam (2017a).

Since the literature review by the authors showed that no researcher provided a study about sandwich microplates with the following given specifications, so the authors motivated to conduct it. The current study is aimed to analyze the vibrational behavior of a small-scale sandwich microplate composed of three layers: an FG-GNPs reinforced composite core and two piezoelectric-reinforced composite faces. The structure was located in a thermal environment and the effect of the temperature variations was assessed. Also, it was rested on the visco-Pasternak type of elastic foundation including springs, shear layer, and dashpots. The GNPs were dispersed along the thickness direction of the plate according to three different patterns. A trigonometric shear deformation theory uses a tangential function to account for the shear deformation effect and is known as the tangential shear deformation theory (TGSDT). Here, TGSDT is utilized to describe the displacement components of the microstructure. Furthermore, the size dependence was taken into account via MSGT with three material length-scale parameters. Hamilton's principle and variational approach were used to derive the governing motion equations which were solved by Navier's technique. The results were verified for the simpler states in the literature and the effect of different materials parameters and geometric sizes of the plate was presented and discussed in detail. The literature review showed no study addressing such a plate. The novelty of the present work lies in considering a three-layered rectangular FG-GNPs reinforced Epoxy microplate which was integrated by piezoelectric-reinforced nanocomposite face sheets and subjected to the electric field in a thermal environment. The findings of this work will help to design and create more optimal engineering and smart structures such as sensors and actuators.

2. Mathematical formulations

As depicted in Fig. 1, a three-layered rectangular microplate is taken into consideration. The core of the microstructure is made from FG-GNPs reinforced Epoxy; while the top and bottom layers are made of piezoelectric-

reinforced single-walled carbon nanotubes (SWCNTs). The externally applied voltage is applied to the faces of the microplate and the structure is rested on a viscoelastic foundation which is simulated by the visco-Pasternak model. The geometrical parameters of the microplate, namely its length, width, and the height of each layer from top to bottom one are shown by L, W, h_t, h_c, and h_b, respectively. Moreover, the total thickness of the structure is shown by h. To analyze the aforementioned microstructure, the Cartesian coordinate system is used whose origin lied at the left corner of the microplate's mid-plane. Also, the displacement components of an arbitrary point of the microplate are described based on a novel TGSDT which uses a tangential function as the shear deformation. This theory can be stated as Amir *et al*. (2020e)

$$\begin{aligned} U(x,y,z,t) &= u(x,y,t) - z\frac{\partial}{\partial x}w_b(x,y,t) \\ &\quad - \Phi(z)w_s(x,y,t), \\ V(x,y,z,t) &= v(x,y,t) - z\frac{\partial}{\partial y}w_b(x,y,t) \\ &\quad - \Phi(z)w_s(x,y,t), \\ W(x,y,z,t) &= w_b(x,y,t) + w_s(x,y,t) \end{aligned} \tag{1}$$

In the above displacement field, the displacements of the mid-layer of the microplate in x and y directions are respectively presented by u and v. Also, the transverse displacements due to bending and shearing are shown by w_b and w_s, respectively. It is noted that $\Phi(z)$ is the shear deformation function which is described based on TGSDT as Amir *et al*. (2020e)

$$\Phi(z) = tan\left(\frac{\pi z}{2h}\right)\zeta^{sec\left(\frac{\pi z}{2h}\right)}, \qquad \zeta = 0.03 \tag{2}$$

The strain components are determined concerning the displacements which lead to the following terms (Brush *et al*. 1975)

$$\begin{aligned} \varepsilon_{xx} &= \frac{\partial u(x,y,t)}{\partial x} - z\frac{\partial^2 w_b(x,y,t)}{\partial x^2} \\ &\quad -\Phi(z)\frac{\partial^2 w_s(x,y,t)}{\partial x^2}, \\ \varepsilon_{yy} &= \frac{\partial v(x,y,t)}{\partial y} - z\frac{\partial^2 w_b(x,y,t)}{\partial y^2} \\ &\quad -\Phi(z)\frac{\partial^2 w_s(x,y,t)}{\partial y^2}, \\ \gamma_{xy} &= \frac{1}{2}\left(\frac{\partial u(x,y,t)}{\partial y} + \frac{\partial v(x,y,t)}{\partial x}\right) \\ &\quad -z\frac{\partial^2 w_b(x,y,t)}{\partial x \partial y} - \Phi(z)\frac{\partial^2 w_s(x,y,t)}{\partial x \partial y}, \\ \gamma_{xz} &= -\frac{1}{2}\left(\Phi_{,z}(z)\frac{\partial w_s(x,y,t)}{\partial x} - \frac{\partial w_s(x,y,t)}{\partial x}\right), \\ \gamma_{yz} &= -\frac{1}{2}\left(\Phi_{,z}(z)\frac{\partial w_s(x,y,t)}{\partial y} - \frac{\partial w_s(x,y,t)}{\partial y}\right) \end{aligned} \tag{3}$$

where comma in subscript denotes the derivative with respect to z.

To derive the governing motion equations, the variational approach and the extended form of Hamilton's principle are used (Cinefra *et al*. 2015)

$$\delta\int_{t_1}^{t_2}(U - T - W)dt = 0 \tag{4}$$

In Eq. (4), U and T are the strain and kinetic energies, respectively and W denotes the work of externally applied loads.

The strain energy of the microplate's core based on the MSGT may be written based on the following expression (Arshid *et al*. 2020a, b)

$$U_c = \frac{1}{2}\int_V \left(\sigma_{ij}\varepsilon_{ij} + p_i\gamma_i + \tau_{ijk}^{(1)}\eta_{ijk}^{(1)} + m_{ij}^{(s)}\chi_{ij}^{(s)}\right)dV \tag{5}$$

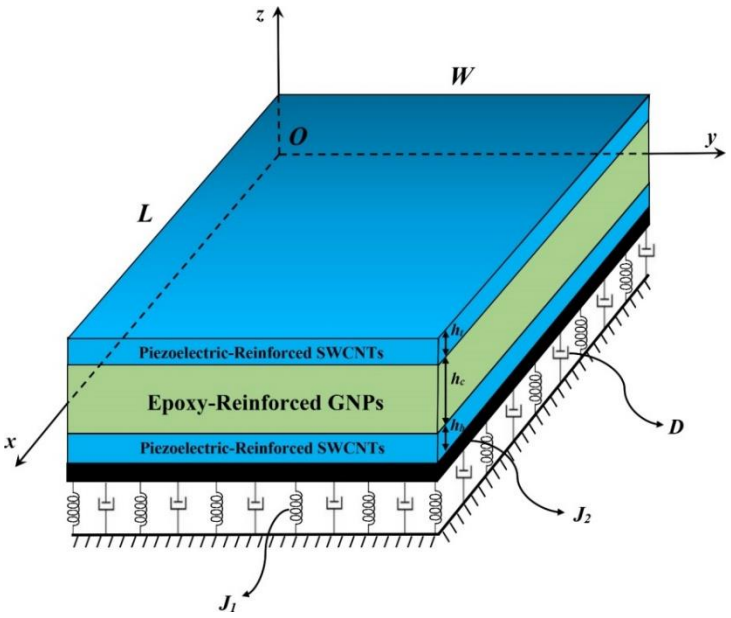

Fig. 1 Schematic diagram of the three-layered microplate on visco-Pasternak substrate

And to calculate its variations, the below relation is obtained

$$\delta U_c = \int_V \left(\sigma_{ij}\delta\varepsilon_{ij} + p_i\delta\gamma_i + \tau_{ijk}^{(1)}\delta\eta_{ijk}^{(1)} + m_{ij}^{(s)}\delta\chi_{ij}^{(s)}\right) dV \quad (6)$$

As noted previously, the MSGT is used to capture the size effect on the vibrational behavior of the under consideration microstructure. In Eq. (6), p_i, $\tau_{ijk}^{(1)}$ and $m_{ij}^{(s)}$ are the higher-order stresses which can be defined as

$$p_i = 2\mu l_0^2\gamma_i, \quad \tau_{ijk}^{(1)} = 2\mu l_1^2\eta_{ijk}^{(1)}, \quad m_{ij}^{(s)} = 2\mu l_2^2\chi_{ij}^{(s)} \quad (7)$$

in the above equations, μ is the Lame's parameter which equals $E/2(1+\nu)$ and δ_{ij} represents Kronecker delta.

Also, l_0, l_1, and l_2 are independent material length-scale parameters which are connected with the dilatation gradients tensor γ_i, deviatoric stretch gradient tensor $\eta_{ijk}^{(1)}$, and symmetric rotation gradients $\chi_{ij}^{(s)}$, respectively with the following forms

$$\gamma_i = \frac{\partial\varepsilon_{mm}}{\partial x}, \quad (8)$$

$$\eta_{ijk}^{(1)} = \frac{1}{3}\left[\left(\frac{\partial\varepsilon_{jk}}{\partial x_i} + \frac{\partial\varepsilon_{ki}}{\partial x_j} + \frac{\partial\varepsilon_{ij}}{\partial x_k}\right),\right.$$
$$-\frac{1}{5}\left(\delta_{ij}\left(\frac{\partial\varepsilon_{mm}}{\partial x_k} + 2\frac{\partial\varepsilon_{mk}}{\partial x_m}\right) + \delta_{jk}\left(\frac{\partial\varepsilon_{mm}}{\partial x_i} + 2\frac{\partial\varepsilon_{mi}}{\partial x_m}\right)\right. \quad (9)$$
$$\left.\left.+\delta_{ki}\left(\frac{\partial\varepsilon_{mm}}{\partial x_j} + 2\frac{\partial\varepsilon_{mj}}{\partial x_m}\right)\right)\right],$$

$$\chi_{ij}^{(s)} = \frac{1}{4}\left(e_{imn}\frac{\partial^2 u_n}{\partial {x_{mj}}^2} + e_{jmn}\frac{\partial^2 u_n}{\partial {x_{mi}}^2}\right) \quad (10)$$

Replacing the displacement components of Eq. (1) in the above equations leads to obtain the components for the dilatation gradients, deviatoric stretch gradient, and the symmetric rotation gradient tensors.

Moreover, the strain energy of the piezoelectric faces can be expressed as (Arshid and Khorshidvand 2018)

$$U_f = \frac{1}{2}\int_V \left(\sigma_{ij}\varepsilon_{ij} + p_i\gamma_i + \tau_{ijk}^{(1)}\eta_{ijk}^{(1)} + m_{ij}^{(s)}\chi_{ij}^{(s)} - D_iE_i\right)dV \quad (11)$$

Similar to the core, variations of the faces, strain energy can be written as

$$\delta U_f = \int_V \left(\sigma_{ij}\delta\varepsilon_{ij} + p_i\delta\gamma_i + \tau_{ijk}^{(1)}\delta\eta_{ijk}^{(1)} + m_{ij}^{(s)}\delta\chi_{ij}^{(s)} - D_i\delta E_i\right) dV \quad (12)$$

where D_i and E_i are electric displacement components and electric field components, respectively that are defined in the next section.

Therefore, summing the Eqs. (6) and (12), the variations of the strain energy for the whole of the microplate are achieved as below

$$\delta U = \delta U_c + \delta U_f$$

$$= \int_A \left\{ \begin{array}{l} \left(\begin{array}{l} -\frac{\partial}{\partial x} N_{xx} - \frac{\partial}{\partial y} N_{xy} - \frac{1}{2}\frac{\partial^2}{\partial y^2} Y_8 - \frac{1}{2}\frac{\partial^2}{\partial y \partial x} Y_{10} + \frac{\partial^2}{\partial x^2} X_1 + \frac{\partial^2}{\partial y \partial x} X_4 + \frac{2}{5}\frac{\partial^2}{\partial x^2} T_1 - \frac{1}{5}\frac{\partial^2}{\partial y^2} T_1 - \frac{2}{5}\frac{\partial^2}{\partial y \partial x} T_5 \\ -\frac{3}{5}\frac{\partial^2}{\partial x^2} T_{11} + \frac{4}{5}\frac{\partial^2}{\partial y^2} T_{11} - \frac{3}{5}\frac{\partial^2}{\partial x^2} T_{19} + \frac{1}{5}\frac{\partial^2}{\partial y^2} T_{19} + \frac{8}{5}\frac{\partial^2}{\partial y \partial x} T_{15} - \frac{2}{5}\frac{\partial^2}{\partial y \partial x} T_{23} \end{array} \right) \delta u + \\ \left(\begin{array}{l} -\frac{\partial}{\partial y} N_{yy} - \frac{\partial}{\partial x} N_{xy} + \frac{1}{2}\frac{\partial^2}{\partial x^2} Y_{10} + \frac{1}{2}\frac{\partial^2}{\partial y \partial x} Y_8 + \frac{\partial^2}{\partial y^2} X_4 + \frac{\partial^2}{\partial y \partial x} X_1 - \frac{2}{5}\frac{\partial^2}{\partial x^2} T_5 + \frac{2}{5}\frac{\partial^2}{\partial y^2} T_5 - \frac{2}{5}\frac{\partial^2}{\partial y \partial x} T_1 \\ -\frac{3}{5}\frac{\partial^2}{\partial y^2} T_{15} + \frac{4}{5}\frac{\partial^2}{\partial x^2} T_{15} - \frac{3}{5}\frac{\partial^2}{\partial y^2} T_{23} - \frac{1}{5}\frac{\partial^2}{\partial x^2} T_{23} + \frac{8}{5}\frac{\partial^2}{\partial y \partial x} T_{11} - \frac{2}{5}\frac{\partial^2}{\partial y \partial x} T_{19} \end{array} \right) \delta v + \\ \left(\begin{array}{l} -2\frac{\partial^2}{\partial y \partial x} T_{32} - \frac{4}{5}\frac{\partial^2}{\partial y^2} T_{29} + \frac{1}{5}\frac{\partial^2}{\partial x^2} T_{29} + \frac{1}{5}\frac{\partial^2}{\partial y^2} T_{27} - \frac{4}{5}\frac{\partial^2}{\partial x^2} T_{27} + \frac{3}{5}\frac{\partial^3}{\partial y \partial x^2} T_{24} + \frac{3}{5}\frac{\partial^3}{\partial y^3} T_{24} \\ -\frac{12}{5}\frac{\partial^3}{\partial y \partial x^2} T_{16} + \frac{3}{5}\frac{\partial^3}{\partial y^3} T_{16} + \frac{3}{5}\frac{\partial^3}{\partial x \partial y^2} T_{20} + \frac{3}{5}\frac{\partial^3}{\partial x^3} T_{20} - \frac{12}{5}\frac{\partial^3}{\partial y^2 \partial x} T_{12} + \frac{3}{5}\frac{\partial^3}{\partial x^3} T_{12} + \frac{1}{5}\frac{\partial^2}{\partial y^2} T_9 \\ +\frac{1}{5}\frac{\partial^2}{\partial x^2} T_9 + \frac{3}{5}\frac{\partial^3}{\partial x^2 \partial y} T_6 - \frac{2}{5}\frac{\partial^3}{\partial y^3} T_6 - \frac{\partial^3}{\partial y^2 \partial x} X_2 - \frac{\partial^3}{\partial y^3} X_5 - \frac{\partial^3}{\partial x^2 \partial y} X_5 - \frac{\partial^2}{dx^2} X_7 - \frac{\partial^2}{\partial y^2} X_7 \\ -\frac{2}{5}\frac{\partial^3}{\partial x^3} T_2 + \frac{3}{5}\frac{\partial^3}{\partial y^2 \partial x} T_2 - \frac{\partial^3}{\partial x^3} X_2 - \frac{\partial^2}{\partial x^2} Y_5 + \frac{\partial^2}{\partial y^2} Y_5 - \frac{\partial^2}{\partial y \partial x} Y_3 + \frac{\partial^2}{\partial y \partial x} Y_1 - 2\frac{\partial^2}{\partial y \partial x} M_{xyb} \\ -\frac{\partial^2}{\partial x^2} M_{xxb} - \frac{\partial^2}{\partial y^2} M_{yyb} \end{array} \right) \delta w_b + \\ \left(\begin{array}{l} \frac{1}{2}\frac{\partial}{\partial x} Y_7 - \frac{1}{2}\frac{\partial^2}{\partial x^2} Y_5 + \frac{1}{2}\frac{\partial^2}{\partial y^2} Y_5 - \frac{1}{2}\frac{\partial^2}{\partial y \partial x} Y_3 + \frac{1}{2}\frac{\partial^2}{\partial y \partial x} Y_1 - \frac{1}{2}\frac{\partial^2}{\partial x^2} Y_6 + \frac{1}{2}\frac{\partial^2}{\partial y^2} Y_6 - \frac{12}{5}\frac{\partial^3}{\partial y^2 \partial x} T_{13} \\ +\frac{3}{5}\frac{\partial^3}{\partial x^3} T_{13} - \frac{1}{2}\frac{\partial^2}{\partial y \partial x} Y_5 + \frac{1}{2}\frac{\partial^2}{\partial y \partial x} Y_3 - \frac{1}{5}\frac{\partial^2}{\partial y^2} T_9 - \frac{1}{5}\frac{\partial^2}{\partial x^2} T_9 - 2\frac{\partial^2}{\partial y \partial x} M_{xys} + \frac{1}{5}\frac{\partial^2}{\partial y^2} T_{10} - \frac{\partial^2}{\partial x^2} M_{xxs} \\ -\frac{\partial^2}{\partial y^2} M_{yys} + \frac{1}{5}\frac{\partial^2}{\partial x^2} T_{10} - \frac{1}{5}\frac{\partial}{\partial y} T_8 + \frac{3}{5}\frac{\partial^3}{\partial x^2 \partial y} T_7 - \frac{2}{5}\frac{\partial^3}{\partial y^3} T_7 - \frac{1}{5}\frac{\partial}{\partial x} T_4 + \frac{3}{5}\frac{\partial^3}{\partial y^2 \partial x} T_3 - \frac{2}{5}\frac{\partial^3}{\partial x^3} T_3 \\ -\frac{\partial^2}{\partial y^2} X_{10} - \frac{1}{5}\frac{\partial}{\partial x} T_{14} - \frac{\partial^2}{\partial x^2} X_8 - \frac{\partial^3}{\partial x^2 \partial y} X_6 - \frac{\partial^3}{\partial y^3} X_6 - \frac{\partial^3}{\partial y^2 \partial x} X_3 - \frac{\partial^3}{\partial x^3} X_3 - 2\frac{\partial^2}{\partial y \partial x} T_{37} \\ +2\frac{\partial^2}{\partial y \partial x} T_{32} + \frac{4}{5}\frac{\partial^2}{\partial y^2} T_{30} - \frac{1}{5}\frac{\partial^2}{\partial x^2} T_{30} - \frac{4}{5}\frac{\partial^2}{\partial y^2} T_{30} + \frac{1}{5}\frac{\partial^2}{\partial x^2} T_{30} - \frac{1}{5}\frac{\partial^2}{\partial y^2} T_{28} + \frac{4}{5}\frac{\partial^2}{\partial x^2} T_{28} + \frac{1}{5}\frac{\partial^2}{\partial y^2} T_{28} \\ -\frac{4}{5}\frac{\partial^2}{\partial x^2} T_{28} + \frac{4}{5}\frac{\partial}{\partial y} T_{26} + \frac{3}{5}\frac{\partial^3}{\partial y \partial x^2} T_{25} + \frac{3}{5}\frac{\partial^3}{\partial y^3} T_{25} - \frac{1}{2}\frac{\partial}{\partial y} Y_{14} - \frac{1}{5}\frac{\partial}{\partial y} T_{18} - \frac{12}{5}\frac{\partial^3}{\partial y \partial x^2} T_{17} + \frac{3}{5}\frac{\partial^3}{\partial y^3} T_{17} \\ +\frac{4}{5}\frac{\partial}{\partial x} T_{22} + \frac{3}{5}\frac{\partial^3}{\partial x \partial y^2} T_{21} + \frac{3}{5}\frac{\partial^3}{\partial x^3} T_{21} \end{array} \right) \delta w_s + \\ \left(\frac{\partial}{\partial x} H_x + \frac{\partial}{\partial y} H_y + H_z \right) \delta \varphi \end{array} \right\} dA \quad (13)$$

in which the used coefficients in Eq. (13) are introduced in "Appendix A".

To calculate the kinetic energy of the under consideration microplate, the following relation may be employed (Ebrahimi *et al*. 2020, Arshid *et al*. 2019b)

$$T = \frac{1}{2}\int_x \int_y \left[\begin{array}{l} \int_{-\frac{h_c}{2}-h_b}^{-\frac{h_c}{2}} \rho \left(\left(\frac{\partial U}{\partial t}\right)^2 + \left(\frac{\partial V}{\partial t}\right)^2 + \left(\frac{\partial W}{\partial t}\right)^2 \right) dz \\ + \int_{-\frac{h_c}{2}}^{\frac{h_c}{2}} \rho(z) \left(\left(\frac{\partial U}{\partial t}\right)^2 + \left(\frac{\partial V}{\partial t}\right)^2 + \left(\frac{\partial W}{\partial t}\right)^2 \right) dz \\ + \int_{\frac{h_c}{2}}^{\frac{h_c}{2}+h_t} \rho \left(\left(\frac{\partial U}{\partial t}\right)^2 + \left(\frac{\partial V}{\partial t}\right)^2 + \left(\frac{\partial W}{\partial t}\right)^2 \right) dz \end{array} \right] dy \, \mathrm{d}x \quad (14)$$

And similar to strain energy, using the variational approach, variations of the kinetic energy may be written as

$$\delta T = \int_x \int_y \left[\begin{array}{l} \left(-I_0 \frac{\partial^2}{\partial t^2} u(x,y,t) + I_1 \frac{\partial^3}{\partial t^2 \partial x} w_b(x,y,t) - I_3 \frac{\partial^2}{\partial t^2} w_s(x,y,t) \right) \delta u + \\ \left(-I_0 \frac{\partial^2}{\partial t^2} v(x,y,t) + I_1 \frac{\partial^3}{\partial y \partial t^2} w_b(x,y,t) - I_3 \frac{\partial^2}{\partial t^2} w_s(x,y,t) \right) \delta v + \\ \left(\begin{array}{l} -I_1 \frac{\partial^3}{\partial t^2 \partial x} u(x,y,t) + I_2 \frac{\partial^4}{\partial t^2 \partial x^2} w_b(x,y,t) - I_4 \frac{\partial^3}{\partial t^2 \partial x} w_s(x,y,t) \\ -I_1 \frac{\partial^3}{\partial t^2 \partial y} v(x,y,t) + I_2 \frac{\partial^4}{\partial t^2 \partial y^2} w_b(x,y,t) - I_4 \frac{\partial^3}{\partial t^2 \partial y} w_s(x,y,t) \\ -I_0 \frac{\partial^2}{\partial t^2} w_b(x,y,t) - I_3 \frac{\partial^2}{\partial t^2} w_s(x,y,t) \end{array} \right) \delta w_b + \\ \left(\begin{array}{l} I_3 \frac{\partial^2}{\partial t^2} u(x,y,t) + I_4 \frac{\partial^3}{\partial t^2 \partial x} w_b(x,y,t) - I_5 \frac{\partial^2}{\partial t^2} w_s(x,y,t) \\ -I_3 \frac{\partial^2}{\partial t^2} v(x,y,t) + I_4 \frac{\partial^3}{\partial t^2 \partial y} w_b(x,y,t) - I_5 \frac{\partial^2}{\partial t^2} w_s(x,y,t) \\ -I_0 \frac{\partial^2}{\partial t^2} w_s(x,y,t) - I_3 \frac{\partial^2}{\partial t^2} w_b(x,y,t) \end{array} \right) \delta w_s \end{array} \right] dy\, dx \quad (15)$$

The used moment inertias (I_i, i = 0, 1,…, 5) are also defined in "Appendix A".

In this paper, the external works included two terms. The first term is due to the viscoelastic substrate, while the second term is attributed to the thermo-electrical loads. Furthermore, as expressed previously, the microstructure was rested on a viscoelastic substrate bearing both normal and shear loads using springs and shear layers, respectively, and also includes dashpots. Consequently, the work of this foundation may be determined via the below equation (Shen *et al*. 2017, Amir *et al*. 2020c)

$$W_s = \frac{1}{2} \int_x \int_y [-F_s(w_b(x,y,t) + w_s(x,y,t))]\, dxdy \quad (16)$$

where the substrate reaction force is presented by F_s that consists of springs, shear layer, and dashpots parameters as follows (Akgöz and Civalek 2018, Amir *et al*. 2020d)

$$\begin{aligned} F_s = {} & J_1\big(w_b(x,y,t) + w_s(x,y,t)\big) \\ & -J_2 \nabla^2\big(w_b(x,y,t) + w_s(x,y,t)\big) \\ & +D(\dot{w}_b(x,y,t) + \dot{w}_s(x,y,t)) \end{aligned} \quad (17)$$

In the above equation, J_1, J_2, and D are substrate parameters relating to the springs, shear layer, and dashpots, respectively. Also, a dot denotes a derivative with respect to time.

The work of thermo-electric load can be evaluated by Eq. (18) (Arshid *et al*. 2019c, Sahmani and Aghdam 2017b)

$$W_{TE} = \frac{1}{2} \int_x \int_y \left\{ \begin{array}{l} \left(\int_{-h/2}^{+h/2} \big(Q_{11}^{c,f} + Q_{12}^{c,f}\big) \alpha_{11}^{c,f} \Delta T dz - 2e_{31}\phi_0 \right) \left(\frac{\partial (w_b(x,y,t) + w_s(x,y,t))}{\partial x} \right)^2 + \\ \left(\int_{-h/2}^{+h/2} \big(Q_{12}^{c,f} + Q_{22}^{c,f}\big) \alpha_{22}^{c,f} \Delta T dz - 2e_{31}\phi_0 \right) \left(\frac{\partial (w_b(x,y,t) + w_s(x,y,t))}{\partial y} \right)^2 \end{array} \right\} dxdy \quad (18)$$

Substituting the obtained expressions for variations of the strain and kinetic energies and also, the work of external loads in Hamilton's principle relation, equating expressions for each coefficient to zero, and rewriting them in terms of displacement components, yields the differential motion equations.

2.1 Constitutive law

As mentioned earlier, the core and the face sheets of the microplate are composed of FG-GNPs reinforced Epoxy and piezoelectric-reinforced SWCNT materials, respectively. To express the strain-stress relations for the core of the structure, the below equation can be used (Kiani 2016, Sahmani *et al*. 2016)

$$\begin{Bmatrix} \sigma_{xx} \\ \sigma_{yy} \\ \gamma_{xy} \\ \gamma_{xz} \\ \gamma_{yz} \end{Bmatrix}^c = \begin{bmatrix} Q_{11c} & Q_{12c} & 0 & 0 & 0 \\ Q_{21c} & Q_{22c} & 0 & 0 & 0 \\ 0 & 0 & Q_{44c} & 0 & 0 \\ 0 & 0 & 0 & Q_{55c} & 0 \\ 0 & 0 & 0 & 0 & Q_{66c} \end{bmatrix} \begin{Bmatrix} \varepsilon_{xx} - \alpha_c(z)\Delta T \\ \varepsilon_{yy} - \alpha_c(z)\Delta T \\ \gamma_{xy} \\ \gamma_{xz} \\ \gamma_{yz} \end{Bmatrix} \quad (19)$$

in which $\alpha_c(z)$ is the thermal expansion coefficient that is the function of thickness, the temperature changes are shown by ΔT, while Q_{ijc} is stiffness components which can be determined via the following relations (Zenkour 2016)

$$\begin{aligned} Q_{iic} &= \frac{(1-\nu_c(z))E_c(z)}{(1+\nu_c(z))(1-2\nu_c(z))}, && i=1,2 \\ Q_{ijc} = Q_{jic} &= \frac{\nu_c(z)E_c(z)}{(1+\nu_c(z))(1-2\nu_c(z))}, && i=1, \quad j=2 \\ Q_{iic} &= \frac{E_c(z)}{2(1+\nu_c(z))}, && i=4,5,6 \end{aligned} \tag{20}$$

It must be noted that the *c* subscript denotes the core. Moreover, $E_c(z)$ and $\nu_c(z)$ are Young's elasticity modulus and the Poisson's ratio of the core, respectively which varied along the thickness direction. To this end, H-T and RM micromechanical models were employed. The previous works showed that the H-T model presents more accurate values for Young's modulus than the other micromechanical models. Therefore, H-T was used to determine the effective Young's elasticity modulus of the core (Yang *et al*. 2018)

$$E_c(z) = \frac{E_M}{8}(3\kappa_1 + 5\kappa_2) \tag{21}$$

where E_M is Young's modulus of the matrix and

$$\kappa_1 = \frac{1+\zeta_L\eta_L V_{GNP}}{1-\eta_L V_{GNP}}, \quad \kappa_2 = \frac{1+\zeta_W\eta_W V_{GNP}}{1-\eta_W V_{GNP}} \tag{22}$$

The used parameters in Eq. (22) which are related to the geometrical properties of the GNPs have the following definitions

$$\zeta_L = 2\frac{l_{GNP}}{h_{GNP}}, \tag{23}$$

$$\eta_W = \frac{(\frac{E_{GNP}}{E_M}) - 1}{(\frac{E_{GNP}}{E_M}) + \zeta_W}, \tag{24}$$

Here, l_{GNP} depicts the GNPs' length, their thickness is shown by h_{GNP} and their width is presented by w_{GNP}. Moreover, E_{GNP} denotes Young's modulus of GNPs reinforcements. The noteworthy, volume fraction of GNPs can be obtained via the following equation

$$V_{GNP} = \frac{g_{GNP}(z)}{g_{GNP}(z) + (\frac{\rho_{GNP}}{\rho_M})(1-g_{GNP}(z))} \tag{25}$$

In the above relation, ρ is the density. The subscripts *GNP* and *M* correspond to the GNPs reinforcements and matrix, respectively. Also, g_{GNP} refers to the weight fraction of reinforcements. If the GNPs dispersed through the core's thickness according to a parabolic function, their weight fraction follows from the below relation (Arefi *et al*. 2019)

$$g_{GNP}(z) = \frac{4}{h_c^2}\beta_1 W_{0GNP} z^2 \tag{26}$$

The values of β_1 which is called the gradient index of GNPs depend on the total GNPs percentage. For 0, 1/3, and 1 percentage of GNPs, the values of β_1 are 0, 1, and 3, respectively.

The linear GNPs dispersion pattern

$$g_{GNP}(z) = \beta_2 W_{0GNP}\left(\frac{1}{2} + \frac{z}{h_c}\right) \tag{27}$$

To determine the values of β_2, for 0, 1/3, and 1 percentage of GNPs, the values of β_2 are 0, 2/3, and 2, respectively.

If GNPs' weight fraction is independent of thickness, then

$$g_{GNP}(z) = \beta_3 W_{0GNP} \tag{28}$$

in which W_{0GNP} is the total mass fraction of GNPs.

For 0, 1/3, and 1 percentage of GNPs, the values of β_3 are 0, 1/3, and 1, respectively.

Moreover, other properties of the face sheets including Poisson's ratio, density, and thermal expansion coefficient can be determined via ERM as follows (Zhong *et al*. 2018)

$$\begin{aligned} \rho_c(z) &= \rho_{GNP}V_{GNP} + \rho_M V_M, \\ \nu_c(z) &= \nu_{GNP}V_{GNP} + \nu_M V_M, \\ \alpha_c(z) &= \alpha_{GNP}V_{GNP} + \alpha_M V_M \end{aligned} \tag{29}$$

Furthermore, the stress-strain relations for piezoelectric-reinforced SWCNT face sheets at the presence of the electric field can be written as (Mohammadimehr *et al*. 2019)

$$\begin{Bmatrix} \sigma_{xx} \\ \sigma_{yy} \\ \sigma_{yz} \\ \sigma_{xz} \\ \sigma_{xy} \end{Bmatrix}^f = \begin{bmatrix} Q_{11f} & Q_{12f} & 0 & 0 & 0 \\ Q_{12f} & Q_{22f} & 0 & 0 & 0 \\ 0 & 0 & Q_{44f} & 0 & 0 \\ 0 & 0 & 0 & Q_{55f} & 0 \\ 0 & 0 & 0 & 0 & Q_{66f} \end{bmatrix} \begin{Bmatrix} \varepsilon_{xx} - \alpha_f \Delta T \\ \varepsilon_{yy} - \alpha_f \Delta T \\ \gamma_{yz} \\ \gamma_{xz} \\ \gamma_{xy} \end{Bmatrix} - \begin{bmatrix} 0 & 0 & e_{31} \\ 0 & 0 & e_{32} \\ 0 & e_{24} & 0 \\ e_{15} & 0 & 0 \\ 0 & 0 & 0 \end{bmatrix} \begin{Bmatrix} E_x \\ E_y \\ E_z \end{Bmatrix} \tag{30}$$

Here, e_{ij} denotes piezoelectric coefficients, the electric field is represented by E_i and Q_{ijf} are stiffness matrix components which can be expressed by

$$\begin{aligned} Q_{11f} &= \frac{E_{11f}(z)}{1-\nu_{12f}\nu_{21f}}, \qquad Q_{22f} = \frac{E_{22f}(z)}{1-\nu_{12f}\nu_{21f}}, \\ Q_{12f} &= \frac{\nu_{21f}E_{11f}(z)}{1-\nu_{21f}\nu_{12f}}, \\ Q_{44f} &= G_{23f}, \qquad Q_{55f} = G_{13f}, \qquad Q_{66f} = G_{12f} \end{aligned} \tag{31}$$

The effective properties of the face sheets can be determined using ERM via the following relations (Paul *et al*. 2013)

$$E_{11f}(z) = \eta_1 V_{CNT} E_{11}^{CNT} + V_m E_m, \tag{32}$$

$$\frac{\eta_2}{E_{22f}(z)} = \frac{V_{CNT}}{E_{22}^{CNT}} + \frac{V_m}{E_m}, \tag{33}$$

matrix.

In the current work, the CNTs are distributed through the thickness of the face sheets according to different functions namely UU, FG-VA, FG-XX, and FG-OO. The first and second letters are related to the top and bottom layers, respectively. The mentioned distribution patterns are related to V_{CNT}^* as follow (Paul *et al*. 2013)

$$V_{CNT}^i = \begin{cases} V_{CNT}^* & \text{UD} \\ \left[1 - \frac{2}{h_i}\left(z \mp \frac{h_c + h_i}{2}\right)\right] V_{CNT}^* & \text{FG-A} \\ \left[1 + \frac{2}{h_i}\left(z \mp \frac{h_c + h_i}{2}\right)\right] V_{CNT}^* & \text{FG-V} \\ 2\left[1 - \frac{2}{h_i}\left(z \mp \frac{h_c + h_i}{2}\right)\right] V_{CNT}^* & \text{FG-O} \\ \frac{4}{h_i}\left[\left|z \mp \frac{h_c + h_i}{2}\right|\right] V_{CNT}^* & \text{FG-X} \end{cases} \quad i = t, b \tag{39}$$

$$\frac{\eta_3}{G_{12f}} = \frac{V_{CNT}}{G_{12}^{CNT}} + \frac{V_m}{G_m} \tag{34}$$

where E_{11}^{CNT}, E_{22}^{CNT}, G_{12}^{CNT}, E_m, and G_m are longitudinal and transverse Young's and shear moduli of the CNTs and matrix, respectively, and $G_{13f} = G_{23f} = G_{12f}$. η_i (i = 1, 2, 3) are efficiency parameters of CNTs which are determined by molecular dynamics (MD) simulation that for $V_{CNT}^* = 0.12$ the efficiency parameters are as $\eta_1 = 0.137$, $\eta_2 = 1.022$, and $\eta_3 = 0.715$. CNTs and matrix volume fraction are shown by V_{CNT} and V_m, respectively, and should be noted that $V_{CNT} + V_m = 1$. It must be noted and that throughout the current paper, that M refers to the matrix of the core and m refers to that of the faces.

The ERM can be developed for other properties of the face sheets, i.e., thermo-electric ones as follow (Hajmohammad *et al*. 2018)

$$P_f = V_{CNT}\{P^{CNT}\} + V_m\{P^m\} \tag{35}$$

where P_f denotes material properties vector and is as follow

$$P_f = \{Q_{ijf}, e_{ij}, \kappa_{ij}, \alpha_{ijf}\} \tag{36}$$

Noted in this study the Poisson's ratio varies through the following relation

$$\nu_{12f} = V_{CNT}^* \nu_{12}^{CNT} + V_m \nu_m \tag{37}$$

The Poisson's ratio is free of different types of CNTs distribution. V_{CNT}^* is the volume fraction of CNTs and defined as follow (Emdadi *et al*. 2019)

$$V_{CNT}^* = \frac{w_{CNT}}{w_{CNT} + \left(\frac{\rho_{CNT}}{\rho_m}\right) - \left(\frac{\rho_{CNT}}{\rho_m}\right) w_{CNT}} \tag{38}$$

in which w_{CNT} denotes the mass density of the CNTs and ρ_{CNT} and ρ_m are densities of the CNTs and the faces' where the negative sign is true for the top and the positive sign is for the bottom face sheets.

Also, the electric displacement can be introduced using the following relation

$$\begin{Bmatrix} D_x \\ D_y \\ D_z \end{Bmatrix} = \begin{bmatrix} 0 & 0 & 0 & e_{15} & 0 \\ 0 & 0 & e_{24} & 0 & 0 \\ e_{31} & e_{32} & 0 & 0 & 0 \end{bmatrix} \begin{Bmatrix} \varepsilon_{xx} \\ \varepsilon_{yy} \\ \gamma_{yz} \\ \gamma_{xz} \\ \gamma_{xy} \end{Bmatrix} + \begin{bmatrix} \kappa_{11} & 0 & 0 \\ 0 & \kappa_{22} & 0 \\ 0 & 0 & \kappa_{33} \end{bmatrix} \begin{Bmatrix} E_x \\ E_y \\ E_z \end{Bmatrix} \tag{40}$$

where κ_{ii} *is* dielectric permeability. To satisfy Maxwell's relations, the electric field can be defined as follow (Arshid *et al*. 2019a)

$$E = -\nabla\Phi \tag{41}$$

The electric and magnetic potentials are the summation of cosine and linear terms (Sobhy 2018)

$$\Phi(x, y, z) = \frac{2z}{h_f}\varphi_0 - cos\left(\frac{\pi z}{h_f}\right)\varphi(x, y) \tag{42}$$

where ϕ_0 is the external applied electric voltage, and h_f shows the thickness of each face sheet. According to Eqs. (41) and (42), the components of the electric field are

$$\begin{aligned} \{E_x, E_y\} &= -\left\{\frac{\partial\Phi}{\partial x}, \frac{\partial\Phi}{\partial y}\right\} = \left\{\frac{\partial\varphi}{\partial x}, \frac{\partial\varphi}{\partial y}\right\} cos\left(\frac{\pi z}{h_f}\right), \\ E_z &= -\frac{\partial\Phi}{\partial z} = -\frac{2}{h_f}\varphi_0 - \frac{\pi}{h_f}\varphi\, sin\left(\frac{\pi z}{h_f}\right) \end{aligned} \tag{43}$$

3. Navier's solution scheme

Based on Navier's solution method which analytically solves the differential equations of the system, the

Table 1 Comparing the results in a simpler state with those of Thai *et al*. (2019)

L/h		Ref.	l_m/h			
			0	**0.2**	**0.4**	**0.8**
5	**Uniform**	**Present**	0.4506	0.5776	0.8356	1.4221
		Thai *et al*. (2019)	0.4437	0.5695	0.8397	1.4922
	Epoxy	**Present**	0.2164	0.2772	0.4016	0.6362
		Thai *et al*. (2019)	0.2132	0.2735	0.4032	0.7163
10	**Uniform**	**Present**	0.1228	0.1532	0.2204	0.3860
		Thai *et al*. (2019)	0.1216	0.1530	0.2220	0.3909
	Epoxy	**Present**	0.0591	0.0737	0.1059	0.1854
		Thai *et al*. (2019)	0.0584	0.0735	0.1066	0.1877

displacements can be considered as functions satisfying the simply supported boundary conditions at the edges of the structure. So, the following functions can be considered for displacement components (Zenkour and Hafed 2020)

$$\begin{Bmatrix} u \\ v \\ w_b \\ w_s \\ \varphi \end{Bmatrix} = \sum_{m=1}^{\infty}\sum_{n=1}^{\infty} \begin{Bmatrix} U\cos(\alpha x)\sin(\beta y) \\ V\sin(\alpha x)\cos(\beta y) \\ W_b\sin(\alpha x)\sin(\beta y) \\ W_s\sin(\alpha x)\sin(\beta y) \\ \Xi\sin(\alpha x)\sin(\beta y) \end{Bmatrix} e^{i\omega t} \quad (44)$$

where U, V, W_b, W_s, and Ξ are amplitudes of displacements and the electric potential of the microplate, respectively. Also, $\alpha = m\pi/L$ and $\beta = n\pi/W$ are the wavenumbers along x and y axes, respectively. Substituting the proposed functions in the governing motion equations, yields

$$([K] + i\omega[C] - \omega^2[M])\{X\} = \{0\} \quad (45a)$$

$$\{X\} = \{u \quad v \quad w_b \quad w_s \quad \varphi\}^T \quad (45b)$$

in which $[K]$, $[C]$, and $[M]$ are the stiffness, damping, and mass matrices, respectively which their arrays are presented in "Appendix B", and ω denotes the natural frequency. Solving Eq. (45a) eigenvalue problem yields the natural frequencies of the structure.

4. Results and discussion

As the first step, the results were compared with the previously published data to ensure their reliability and accuracy. To this end, since the present work is the first analysis with the aforementioned specifications and there is no similar work in the open literature, the authors neglected some parameters to make the results comparable to other papers. Therefore, the dimensionless natural frequencies for a rectangular FG-GNPs reinforced composites microplate were obtained and compared with those of Thai *et al*. (2019). To extract the results, the thicknesses of the faces were set to zero implying that the results were obtained for an FG-GNPs reinforced microplate according to MCST and MSGT. Moreover, the effects of the foundation and thermal environment were not included in this part. The results were presented for two cases, namely pure Epoxy and uniform

Table 2 Thermo-mechanical properties of the GNPs-reinforced Epoxy core (Amir *et al*. 2020b)

Properties	GNPs reinforcement	Epoxy matrix
E	1.01 TPa	3 GPa
ρ	1062.5 kg/m^3	1200 kg/m^3
v	0.186	0.34
l	2.5 μm	-
w	1.5 μm	-
h	1.5 nm	-
α	2.35×10^{-5} K^{-1}	8.2×10^{-5} K^{-1}

Table 3 Thermo-mechanical properties of the piezoelectric-reinforced SWCNTs faces (Arshid *et al*. 2020a, Amir *et al*. 2020b)

Properties	SWCNTs reinforcements	PVDF matrix
E_{11}	5.64 TPa	2.2 GPa
E_{22}	7.08 TPa	-
G_{12}	1.9445 TPa	-
ρ	1400 kg/m^3	1780 kg/m^3
v	0.175	0.384
e_{31}	0	-0.13 C/m^2
e_{32}	0	-0.45 C/m^2
e_{15}	0	-0.009 C/m^2
κ_{11}= κ_{22}	0	0.1107 nF/m
κ_{33}	0	0.1061 nF/m
α_{11}	3.4584×10^{-6} K^{-1}	4.1682×10^{-6} K^{-1}
α_{22}	5.1682×10^{-6} K^{-1}	-

GNPs dispersion pattern and also, for different l_m/h and L/h ratios. According to Table 1, the current results and those of Thai *et al*. (2019) coincided suggesting a good agreement. The dimensionless natural frequency in Table 1 is defined as $\Omega = (\omega L^2/h)\sqrt{\rho_m/E_m}$. Noteworthy, the slight difference between the results can be due to differences in displacement field theories used by Thai *et al*. (2019) and the present study and also, the different approaches used to solve the differential equations. Therefore, the results and their accuracy are verified. In the following, the results regarding all of the parameters are presented. The thermo-

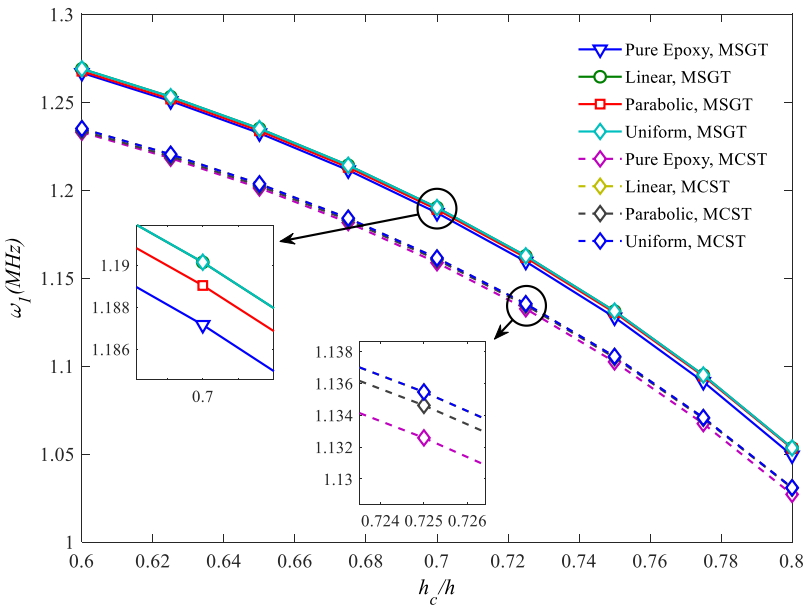

Fig. 2 Effect of thicknesses ratio for different values of GNPs based on MCS and MSG theories on the first natural frequency

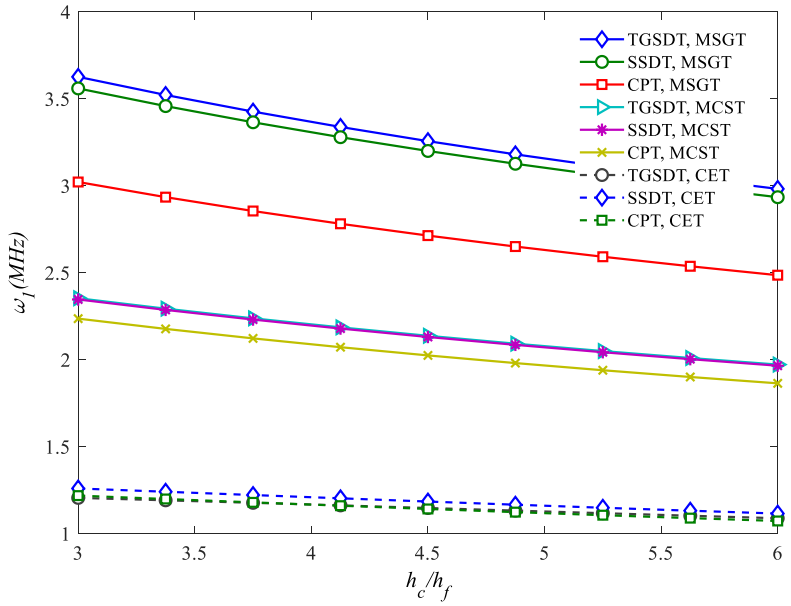

Fig. 3 Investigation of the effect of different theories on the fundamental natural frequency of the microplate

mechanical properties of the core and the faces are presented in Tables 2 and 3 (Arshid *et al*. 2020a, b, Amir *et al*. 2020b). Moreover, the total height of the microplate was taken 150 μm and the length-scale parameters, i.e., l_0, l_1, and l_2 were set equal to each other (l_m), ten times smaller than h. Also, the core's and faces' thickness is $0.8h$ and $0.1h$, respectively. It must be noted that for all of the following graphs, unless otherwise expressed, the length and width of the microplate are equal to each other ($L = W = 10h$) and the distribution patterns of GNPs and CNTs are uniform.

In the next step, the results are presented and discussed in detail in the following. Fig. 2 shows the impact of different parameters on the fundamental natural frequency of the investigated microplate. Based on Fig. 2, an increase in the core-to-total thicknesses ratio led to a reduction in the natural frequency due to a reduction in the microstructure's stiffness. The results in Fig. 2 are presented based on both MCS and MSG theories. Generally, the MSGT results are larger than MCST ones which might be because MSGT uses three length-scale parameters and takes the dilatation and deviatoric stretch gradient strains into account (instead of only symmetric rotation gradient as in the MCST. Moreover, the pure Epoxy core exhibited smaller natural frequencies in comparison to other GNPs-reinforced cases regardless of their dispersion patterns. A comparison of different types of GNPs dispersion shows that uniform and parabolic distribution patterns led to the most and the least natural frequencies, respectively. In Fig. 3, in addition to the thicknesses ratio, the effect of different shear deformation theories, namely TGSDT, SSDT, and CPT in micro and

macro scales is investigated. As depicted in Fig. 3, TGSDT leads to the larger values of frequency in comparison with the two other theories, i.e., SSDT and CPT. As previously stated, MSGT-based structure had higher natural frequencies compared to MCST-based ones. It must be noted that the frequencies of the macro plate (that can be obtained by setting the length-scale parameters to zero) are generally lower than their macro peers. Furthermore, enhancing the core to face thickness ratio made the microstructure softer, and accordingly, its natural frequency tended to reduce.

The effects of temperature variations and also, the dimensionless length-scale parameter on the fundamental natural frequency is depicted in Fig. 4. An increase in the temperature enhanced the structure's softness and declined its natural frequency. Also, an enhancement in the dimensionless length-scale parameter makes the structure stiffer and thus raised the natural frequency. As suggested by Fig. 4 and previous discussions, the results of the macro plate obtained based on CET were independent of the variations of the length-scale parameter.

The influence of h_c/L on the results is shown in Fig. 5 for different conditions. An increase in the core's thickness respective to the microplate's length (by keeping the total thickness constant) caused more vibration in the structure implying smaller natural frequencies. It occurred due to a reduction in the microstructure's stiffness.

As mentioned before, the piezoelectric face sheets were

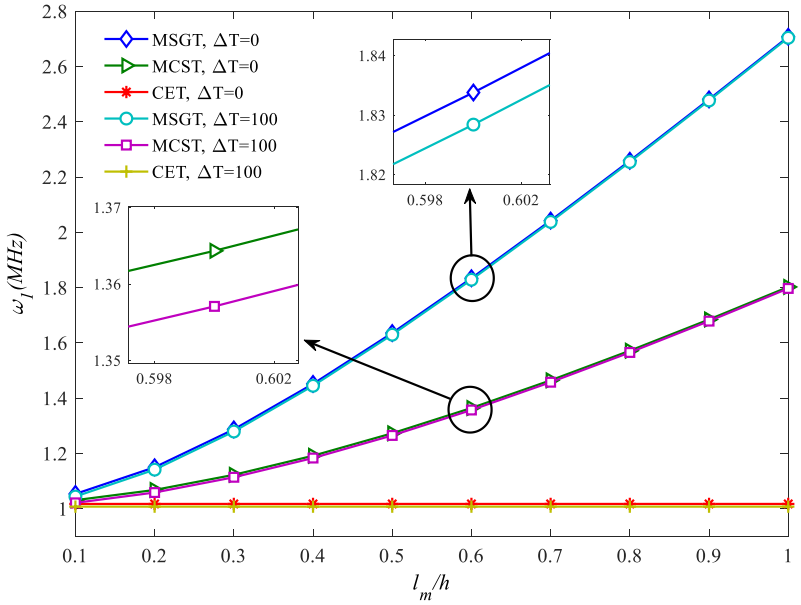

Fig. 4 Length-scale parameter effect for different temperature changes on the results

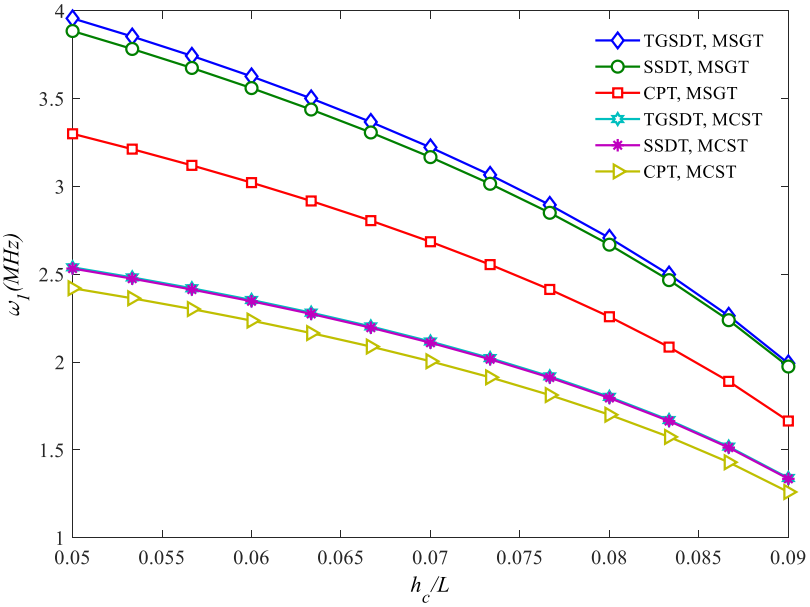

Fig. 5 Height-to-length ratio influence on the natural frequency of the microplate

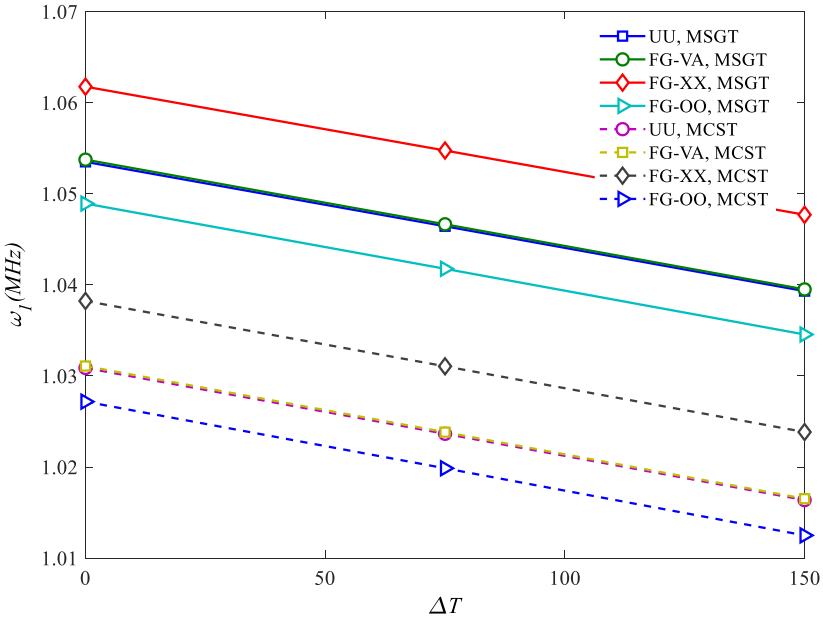

Fig. 6 CNTs distribution pattern effect based on temperature changes on the natural frequency

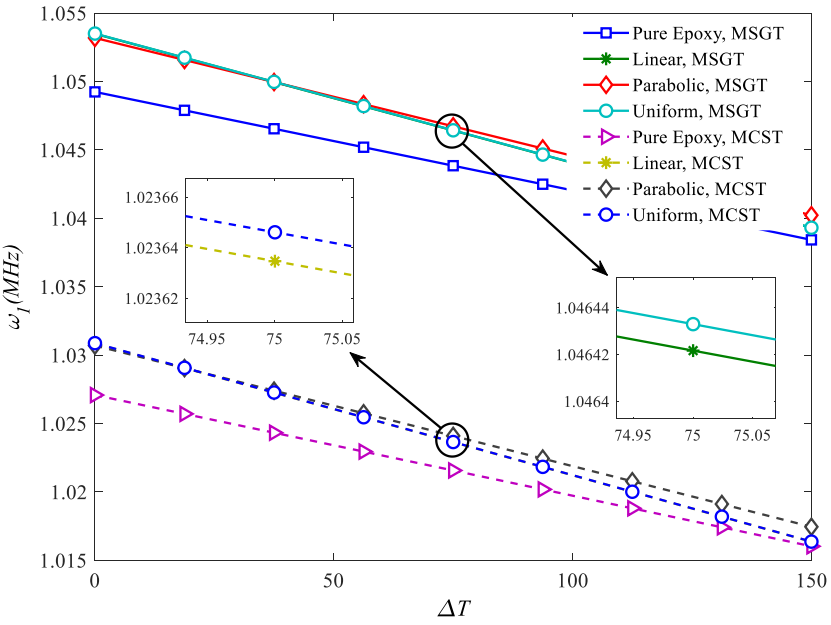

Fig. 7 GNPs dispersion pattern effect on the results

reinforced by SWCNTs through different distribution patterns as mentioned in Eq. (39). Fig. 6 illustrates the effects of different CNTs distribution patterns and also the temperature variations on the results. According to Fig. 6, among the considered patterns, FG-XX and FG-OO led to the highest and the lowest frequencies, respectively. In the FG-XX pattern, the CNTs were more distributed on the surfaces rather than the mid-plane and. The inverse condition held for the FG-OO which affected the results. Fig. 6 also confirms the previous findings stating that an elevation of temperature enhances the structure softness and accordingly, reduces the natural frequency.

Fig. 7 considers a similar effect but for GNPs. As can beseen, by increasing the temperature from zero to 150, the natural frequencies were declined. Moreover, MSGT and MCST results were significantly different.

Tables 4 and 5 list the exact natural frequencies for different shapes, l_m/h, and L/h ratios. It can be found that an increase in the dimensionless length-scale parameter raised the natural frequencies. Table 4 is related to the rectangular microplate, while Table 5 is for a square one. As we know, the results of the rectangular microplate are generally higher than the square plate, in the same area. A comparison between these two tables showed that these results are not obtained

Table 4 Effect of length-scale parameter and length to thickness ratio of the rectangular microplate on the natural frequencies of different modes (ΔT = 20)

L/h		(m, n)	l_m/h				
			0	**0.2**	**0.6**	**0.8**	**1**
10	**MSGT**	**(1,1)**	0.7227	0.8386	1.3342	1.6444	1.9720
		(2,1)	2.0497	1.5661	2.5121	3.0933	3.6398
		(2,2)	2.7264	3.2419	5.0828	5.4107	5.5819
	MCST	**(1,1)**	0.7227	0.7579	0.9735	1.1252	1.2939
		(2,1)	2.0497	2.1□27	2.8859	3.3568	3.8752
		(2,2)	2.7264	2.9115	3.8210	4.4187	5.0777
20	**MSGT**	**(1,1)**	0.3533	0.3974	0.6418	0.7951	0.9566
		(2,1)	0.9705	1.1102	1.8232	2.2611	2.7213
		(2,2)	1.3743	1.5661	2.5121	3.0933	3.6398
	MCST	**(1,1)**	0.3533	0.3690	0.4710	0.5440	0.6253
		(2,1)	0.9705	1.0231	1.3349	1.5512	1.7905
		(2,2)	1.3743	1.4492	1.8699	2.1594	2.4806

Table 5 Effect of length-scale parameter and length to thickness ratio of the square microplate on the natural frequencies of different modes (ΔT = 20)

L/h		(m, n)	l_m/h				
			0	**0.2**	**0.6**	**0.8**	**1**
10	**MSGT**	**(1,1)**	1.0154	1.1482	1.8327	2.2578	2.7066
		(2,1)	2.3401	2.7138	4.3660	5.0824	5.2268
		(2,2)	1.0154	4.3909	6.1475	6.3740	6.6531
	MCST	**(1,1)**	1.0154	1.0660	1.3629	1.5703	1.8013
		(2,1)	2.3401	2.4940	3.2812	3.8044	4.3811
		(2,2)	1.0154	4.0325	5.3090	6.1215	6.5506
20	**MSGT**	**(1,1)**	0.2586	0.2897	0.4649	0.5753	0.6918
		(2,1)	0.6149	0.6977	1.1395	1.4136	1.7019
		(2,2)	1.0154	1.1482	1.8327	2.2578	2.7066
	MCST	**(1,1)**	0.2586	0.2696	0.3421	0.3943	0.4526
		(2,1)	0.6149	0.6452	0.8335	0.9662	1.1134
		(2,2)	1.0154	1.0660	1.3629	1.5703	1.8013

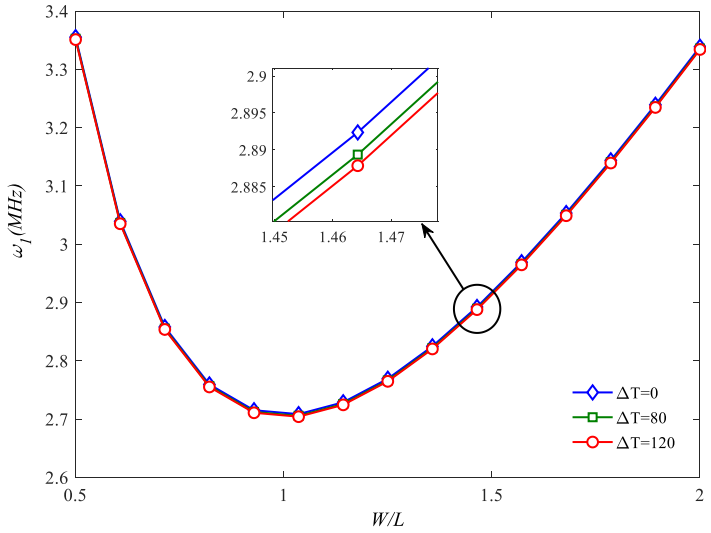

Fig. 8 Aspect ratio of the microplate effect on its natural frequency

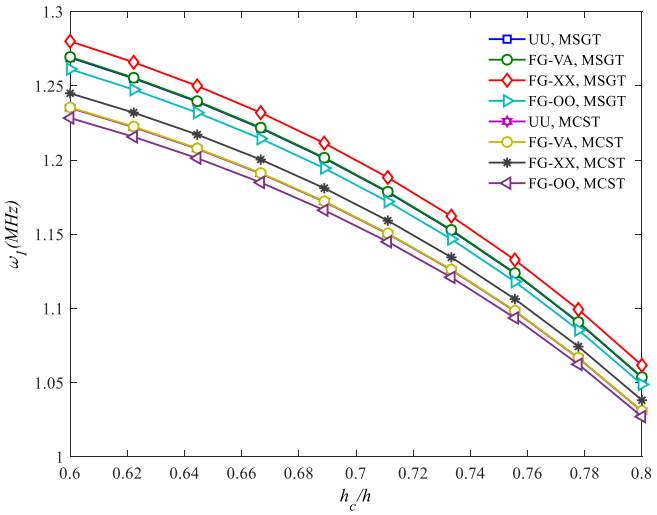

Fig. 9 Core's to total thickness ratio influence on the results based on MCS and MSG theories and different patterns of CNTs distribution

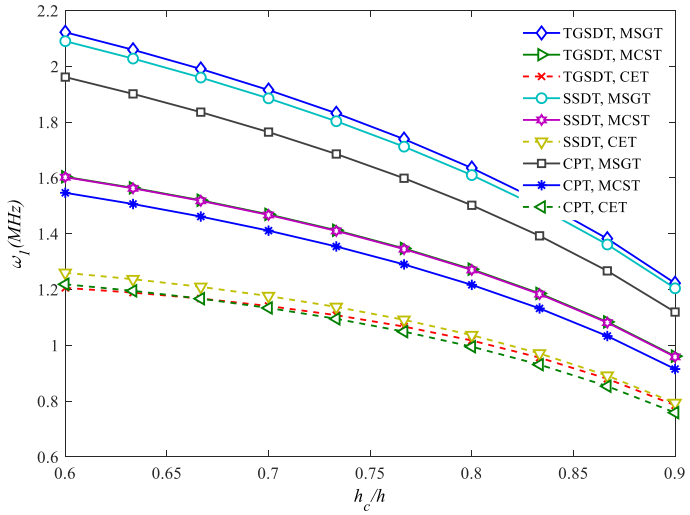

Fig. 10 Comparing the effect of different shear deformation theories on micro and macro plates' natural frequencies

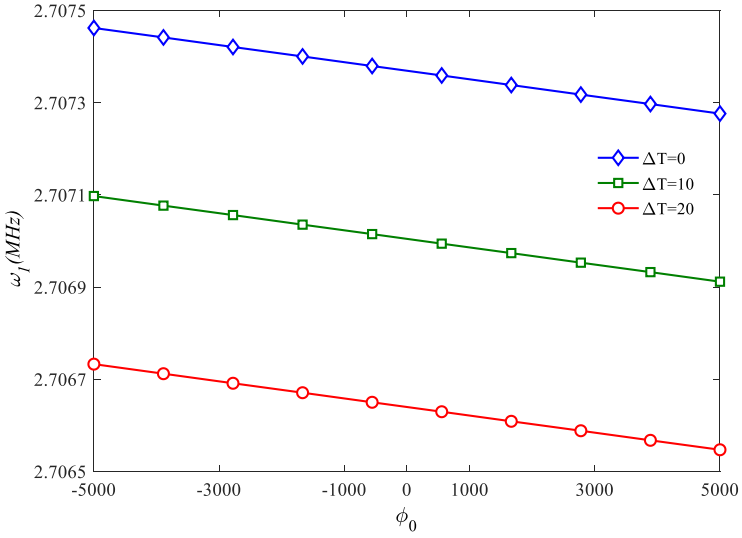

Fig. 11 Effect of the externally applied voltage to the piezoelectric faces on the results

as the areas in the mentioned two tables are not equal.

Fig. 8 presents the effect of the aspect ratio of the microplate on its natural frequency. When the length and width of the microplate are equals, i.e., when the rectangular plate converts to a square one, the natural frequency is in its minimum values. But in other cases, i.e., rectangular plate with any aspect ratio value, the natural frequencies are higher than that of the square microplate.

In Fig. 9, the effect of CNTs distribution patterns versus the thicknesses ratio is considered. Similar to previous graphs, maximum natural frequencies were observed in the FG-XX pattern, while the minimum values were for the FG-OO pattern.

The horizontal axis in Fig. 10 shows the thickness ratio, while the curves of this figure are plotted based on different theories for both micro and macro-scaled structures.

Fig. 11 depicts the effect of an external voltage applied to the piezoelectric faces on the fundamental natural frequency of the microplate. An increase in the applied voltage declined the natural frequency due to a reduction in the stiffness of the microstructure as a result of the polarization phenomena.

The simultaneous effects of temperature and external voltage are illustrated in Fig. 12 in a 3-D plot. As can be seen, the enhancement of both these parameters led to the reduction of the first natural frequency of the microplate.

Different models of the elastic substrate are compared in Fig. 13. Noteworthy, the substrate which just includes springs is called Winkler; the one including both springs and the shear layer is called Pasternak, while the one encompassing dashpots in addition to springs ad shear layer is called visco-Pasternak. As can be seen in Fig. 13, neglecting the substrate form makes the natural frequency less than other types. Adding the elastic substrate, regardless of its type, increased the rigidity of the structure and accordingly, enhanced the results. Comparing the Winkler and Pasternak models, the Pasternak leads to higher natural frequencies due to including a shear layer.

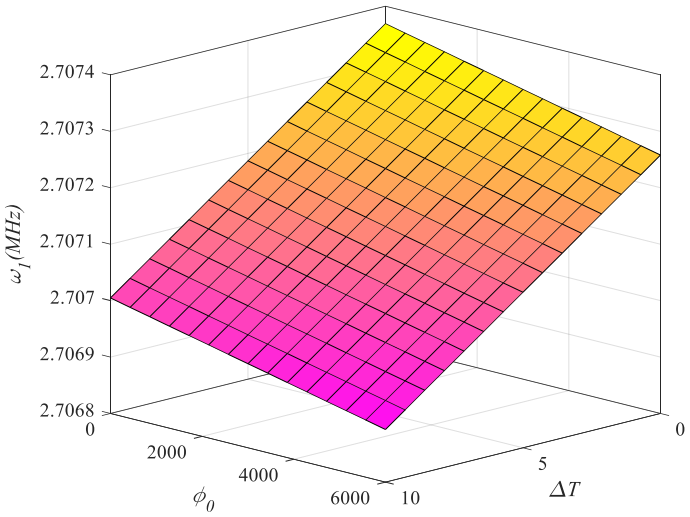

Fig. 12 Simultaneously consideration on the effect of temperature and applied voltage on the fundamental natural frequency of the microplate

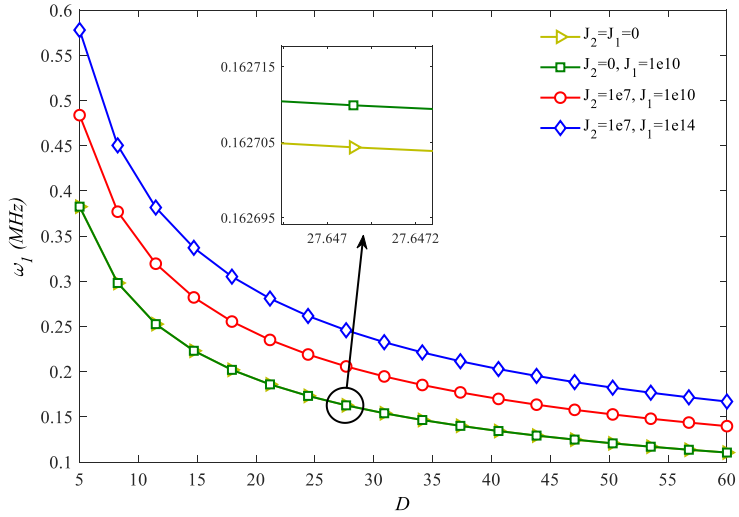

Fig. 13 Comparing different models of the elastic substrate and their parameters influence on the natural frequency of the microplate

Unlike the springs and shear layer parameters, adding the dashpots and increasing the dashpots' parameters reduced the microplate's rigidity and decreased the results.

5. Conclusions

In the current study, vibration characteristics of a three-layered rectangular microplate with GNPs-reinforced Epoxy core which is fully bonded to piezoelectric-reinforced SWCNTs patches are provided. The face sheets are subjected to the electric field and the microplate is assumed to be in a thermal environment. Also, it is located on the visco-Pasternak model of the elastic substrate. To account the shear deformation effect, TGSDT as a higher-order theory is employed and MSGT with tree length-scale parameters is selected to capture the size effect. Using the extended form of Hamilton's principle and variational formulation, the governing motion equations were derived and solved mathematically. The results were validated with the known data in the literature and the following items are concluded:

- Adding the GNPs to the Epoxy matrix of the core, tends the natural frequencies to enhance.
- Among different patterns of GNPs dispersion, linear and parabolic patterns lead to the most and the least natural frequencies, respectively.
- Comparing different patterns of CNTs distribution along with the faces' thickness shows that FG-XX and FG-OO lead to the maximum and minimum values of natural frequencies.
- Increasing the externally applied voltage to the faces, makes the structure softer and accordingly, leads the natural frequencies to reduce.
- The results predicted by MSGT are generally higher than those predicted by MCST due to additional length-scale parameters and considered effects.
- Increasing the temperature rather than the ambient one leads the results to reduce due to a reduction in microplate's stiffness.
- Adding the elastic substrate, regardless of its type, makes the microstructures' rigidity more and accordingly, leads the frequencies to enhance.
- Although increasing both springs and shear layer parameters leads the natural frequencies to increase, but enhancing the dashpots parameter tends them to reduce.

References

Abazid, M.A. (2019), "The Nonlocal Strain Gradient Theory for Hygrothermo-Electromagnetic Effects on Buckling, Vibration and Wave Propagation in Piezoelectromagnetic Nanoplates", *Int. J. Appl. Mech.*, **11**(7), 1950067. https://doi.org/10.1142/S1758825119500674

Akgöz, B. and Civalek, Ö. (2018), "Vibrational characteristics of embedded microbeams lying on a two-parameter elastic foundation in thermal environment", *Compos. Part B: Eng.*, **150**, 68-77. https://doi.org/10.1016/j.compositesb.2018.05.049

Allahkarami, F. and Nikkhah-Bahrami, M. (2018), "The effects of agglomerated CNTs as reinforcement on the size-dependent vibration of embedded curved microbeams based on modified couple stress theory", *Mech. Adv. Mater. Struct.*, **25**(12), 995-1008. https://doi.org/10.1080/15376494.2017.1323144

Amir, S., Khorasani, M. and BabaAkbar-Zarei, H. (2018), "Buckling analysis of nanocomposite sandwich plates with piezoelectric face sheets based on flexoelectricity and first-order shear deformation theory", *J. Sandw. Struct. Mater.*, 109963621879538. https://doi.org/10.1177/1099636218795385

Amir, S., Arshid, E. and Ghorbanpour Arani, M.R. (2019a), "Size-dependent magneto-electro-elastic vibration analysis of FG saturated porous annular/ circular micro sandwich plates embedded with nano-composite face sheets subjected to multi-physical pre loads", *Smart Struct. Syst.*, **23**(5), 429-447. https://doi.org/10.12989/sss.2019.23.5.429

Amir, S., Soleimani-Javid, Z. and Arshid, E. (2019b), "Size-dependent free vibration of sandwich micro beam with porous core subjected to thermal load based on SSDBT", *ZAMM Zeitschrift Fur Angewandte Mathematik Und Mechanik*, **99**(9), 1-21. https://doi.org/10.1002/zamm.201800334

Amir, S., Bidgoli, E.M.R. and Arshid, E. (2020a), "Size-dependent vibration analysis of a three-layered porous rectangular nano plate with piezo-electromagnetic face sheets subjected to pre loads based on SSDT", *Mech. Adv. Mater. Struct.*, **27**(8), 605-619. https://doi.org/10.1080/15376494.2018.1487612

Amir, S., Vossough, A.R., Vossough, H. and Arshid, E. (2020b), "Nonlinear magneto-nonlocal vibration analysis of coupled piezoelectric micro-plates reinforced with agglomerated CNTs", *Mech. Adv. Compos. Struct.*, **7**(1), 109-119. https://doi.org/10.22075/macs.2019.16632.1185

Amir, S., Arshid, E. and Khoddami Maraghi, Z. (2020c), "Free vibration analysis of magneto-rheological smart annular three-layered plates subjected to magnetic field in viscoelastic medium", *Smart Struct. Syst.*, **25**(5), 581-592. https://doi.org/10.12989/sss.2020.25.5.581

Amir, S., Arshid, E., Khoddami Maraghi, Z., Loghman, A. and Ghorbanpour Arani, A. (2020d), "Vibration analysis of magnetorheological fluid circular sandwich plates with magnetostrictive facesheets exposed to monotonic magnetic field located on visco-Pasternak substrate", *JVC/J. Vib. Control*, **26**(17-18), 1523-1537. https://doi.org/10.1177/1077546319899203

Amir, S., Arshid, E., Rasti-Alhosseini, S.M.A. and Loghman, A. (2020e), "Quasi-3D tangential shear deformation theory for size-dependent free vibration analysis of three-layered FG porous micro rectangular plate integrated by nano-composite faces in hygrothermal environment", *J. Thermal Stress.*, **43**(2), 133-156. https://doi.org/10.1080/01495739.2019.1660601

Arefi, M., Mohammad-Rezaei Bidgoli, E. and Rabczuk, T. (2019), "Thermo-mechanical buckling behavior of FG GNP reinforced micro plate based on MSGT", *Thin-Wall. Struct.*, **142**, 444-459. https://doi.org/10.1016/j.tws.2019.04.054

Arshid, E. and Khorshidvand, A.R. (2018), "Free vibration analysis of saturated porous FG circular plates integrated with piezoelectric actuators via differential quadrature method", *Thin-Wall. Struct.*, **125**, 220-233. https://doi.org/10.1016/j.tws.2018.01.007

Arshid, E., Kiani, A. and Amir, S. (2019a), "Magneto-electro-elastic vibration of moderately thick FG annular plates subjected to multi physical loads in thermal environment using GDQ method by considering neutral surface", *Proceedings of the Institution of Mechanical Engineers, Part L: Journal of Materials: Design and Applications*, **233**(10), 2140-2159. https://doi.org/10.1177/1464420719832626

Arshid, E., Khorshidvand, A.R. and Khorsandijou, S.M. (2019b), "The effect of porosity on free vibration of SPFG circular plates resting on visco-Pasternak elastic foundation based on CPT,

FSDT and TSDT", *Struct. Eng. Mech.*, *Int. J.*, **70**(1), 97-112. https://doi.org/10.12989/sem.2019.70.1.097

Arshid, E., Kiani, A., Amir, S. and Zarghami Dehaghani, M. (2019c), "Asymmetric free vibration analysis of first-order shear deformable functionally graded magneto-electro-thermo-elastic circular plates", *Proceedings of the Institution of Mechanical Engineers, Part C: Journal of Mechanical Engineering Science*, **233**(16), 5659-5675. https://doi.org/10.1177/0954406219850598

Arshid, E., Amir, S. and Loghman, A. (2020a), "Static and dynamic analyses of FG-GNPs reinforced porous nanocomposite annular micro-plates based on MSGT", *Int. J. Mech. Sci.*, **180**, 105656. https://doi.org/10.1016/j.ijmecsci.2020.105656

Arshid, E., Amir, S. and Loghman, A. (2020b), "Bending and buckling behaviors of heterogeneous temperature-dependent micro annular/circular porous sandwich plates integrated by FGPEM nano-Composite layers", *J. Sandw. Struct. Mater.*, 109963622095502. https://doi.org/10.1177/1099636220955027

Behdinan, K., Moradi-Dastjerdi, R., Safaei, B., Qin, Z., Chu, F. and Hui, D. (2020), "Graphene and CNT impact on heat transfer response of nanocomposite cylinders", *Nanotechnol. Reviews*, **9**(1), 41-52. https://doi.org/10.1515/ntrev-2020-0004

Brush, D.O., Almroth, B.O. and Hutchinson, J.W. (1975), "Buckling of bars, plates, and shells", *J. Appl. Mech.*, **42**, 911. https://doi.org/10.1115/1.3423755

Chikr, S.C., Kaci, A., Bousahla, A.A., Bourada, F., Tounsi, A., Bedia, E.A. and Tounsi, A. (2020), "A novel four-unknown integral model for buckling response of FG sandwich plates resting on elastic foundations under various boundary conditions using Galerkin's approach", *Geomech. Eng.*, **21**(5), 471-487. https://doi.org/10.12989/GAE.2020.21.5.471

Cinefra, M., Valvano, S. and Carrera, E. (2015), "A layer-wise MITC9 finite element for the free-vibration analysis of plates with piezo-patches", *Int. J. Smart Nano Mater.*, **6**(2), 85-104. https://doi.org/10.1080/19475411.2015.1037377

Duc, N.D. (2018), "Nonlinear thermo-electro-mechanical dynamic response of shear deformable piezoelectric sigmoid functionally graded sandwich circular cylindrical shells on elastic foundations", *J. Sandw. Struct. Mater.*, **20**(3), 351-378. https://doi.org/10.1177/1099636216653266

Ebrahimi, F., Karimiasl, M. and Selvamani, R. (2020), "Bending analysis of magneto-electro piezoelectric nanobeams system under hygro-thermal loading", *Adv. Nano Res.*, **8**(3), 203-214. https://doi.org/10.12989/anr.2020.8.3.203

Emdadi, M., Mohammadimehr, M. and Navi, B.R. (2019), "Free vibration of an annular sandwich plate with CNTRC facesheets and FG porous cores using Ritz method", *Adv. Nano Res.*, **7**(2), 109-123. https://doi.org/10.12989/anr.2019.7.2.109

Eringen, A.C. (1983), "On differential equations of nonlocal elasticity and solutions of screw dislocation and surface waves", *J. Appl. Phys.*, **54**(9), 4703-4710. https://doi.org/10.1063/1.332803

Eringen, A.C. (2002), *Nonlocal Continuum Field Theories*, Springer Science & Business Media. https://doi.org/10.1007/b97697

Eyvazian, A., Shahsavari, D. and Karami, B. (2020), "On the dynamic of graphene reinforced nanocomposite cylindrical shells subjected to a moving harmonic load", *Int. J. Eng. Sci.*, **154**, 103339. https://doi.org/10.1016/j.ijengsci.2020.103339

Fattahi, A.M., Safaei, B. and Moaddab, E. (2019a), "The application of nonlocal elasticity to determine vibrational behavior of FG nanoplates", *Steel Compos. Struct.*, **32**(2), 281-292. https://doi.org/10.12989/scs.2019.32.2.281

Fattahi, A.M., Safaei, B. and Ahmed, N.A. (2019b), "A comparison for the non-classical plate model based on axial buckling of single-layered graphene sheets", *Eur. Phys. J. Plus*, **134**(11), 1-13. https://doi.org/10.1140/epjp/i2019-12912-7

Ferreira, A.J.M., Fasshauer, G.E., Batra, R.C. and Rodrigues, J.D. (2008), "Static deformations and vibration analysis of composite and sandwich plates using a layerwise theory and RBF-PS discretizations with optimal shape parameter", *Compos. Struct.*, **86**(4), 328-343. https://doi.org/10.1016/J.COMPSTRUCT.2008.07.025

García-Macías, E., Rodríguez-Tembleque, L. and Sáez, A. (2018), "Bending and free vibration analysis of functionally graded graphene vs. carbon nanotube reinforced composite plates", *Compos. Struct.*, **186**, 123-138. https://doi.org/10.1016/j.compstruct.2017.11.076

Habibi, M., Taghdir, A. and Safarpour, H. (2019), "Stability analysis of an electrically cylindrical nanoshell reinforced with graphene nanoplatelets", *Compos. Part B: Eng.*, **175**, 107125. https://doi.org/10.1016/j.compositesb.2019.107125

Hajmohammad, M.H., Zarei, M.S., Farrokhian, A. and Kolahchi, R. (2018), "A layerwise theory for buckling analysis of truncated conical shells reinforced by CNTs and carbon fibers integrated with piezoelectric layers in hygrothermal environment", *Adv. Nano Res.*, **6**(4), 299-321. https://doi.org/10.12989/anr.2018.6.4.299

Iijima, S. (1991), "Helical microtubules of graphitic carbon", *Nature*, **354**(6348), 56. https://doi.org/10.1038/354056a0

Karami, B. and Shahsavari, D. (2020), "On the forced resonant vibration analysis of functionally graded polymer composite doubly-curved nanoshells reinforced with graphene-nanoplatelets", *Comput. Methods Appl. Mech. Eng.*, **359**, 112767. https://doi.org/10.1016/j.cma.2019.112767

Karami, B., Shahsavari, D. and Janghorban, M. (2018), "A comprehensive analytical study on functionally graded carbon nanotube-reinforced composite plates", *Aerosp. Sci. Technol.*, **82-83**, 499-512. https://doi.org/10.1016/j.ast.2018.10.001

Karami, B., Janghorban, M. and Tounsi, A. (2019a), "Galerkin's approach for buckling analysis of functionally graded anisotropic nanoplates/different boundary conditions", *Eng. Comput.*, **35**(4), 1297-1316. https://doi.org/10.1007/s00366-018-0664-9

Karami, B., Janghorban, M. and Tounsi, A. (2019b), "On exact wave propagation analysis of triclinic material using three-dimensional bi-Helmholtz gradient plate model", *Struct. Eng. Mech., Int. J.*, **69**(5), 487-497. https://doi.org/10.12989/sem.2019.69.5.487

Karami, B., Janghorban, M. and Tounsi, A. (2019c), "Wave propagation of functionally graded anisotropic nanoplates resting on Winkler-Pasternak foundation", *Struct. Eng. Mech.*, **70**(1), 55-66. https://doi.org/10.12989/sem.2019.70.1.055

Karami, B., Shahsavari, D., Janghorban, M. and Li, L. (2019d), "Elastic guided waves in fully-clamped functionally graded carbon nanotube-reinforced composite plates", *Mater. Res. Express*, **6**(9), 0950a9. https://doi.org/10.1088/2053-1591/ab3474

Karami, B., Shahsavari, D., Janghorban, M. and Li, L. (2019e), "Influence of homogenization schemes on vibration of functionally graded curved microbeams", *Compos. Struct.*, **216**, 67-79. https://doi.org/10.1016/j.compstruct.2019.02.089

Karami, B., Shahsavari, D., Janghorban, M. and Tounsi, A. (2019f), "Resonance behavior of functionally graded polymer composite nanoplates reinforced with graphene nanoplatelets", *Int. J. Mech. Sci.*, **156**, 94-105. https://doi.org/10.1016/j.ijmecsci.2019.03.036

Karami, B., Gheisari, P., Nazemosadat, S.M.R., Akbari, P., Shahsavari, D., Naghizadeh, M. and Naghizadeh, M. (2020), "Elastic wave characteristics of graphene nanoplatelets reinforced composite nanoplates", *Struct. Eng. Mech.*, **74**(6), 809-819. https://doi.org/10.12989/sem.2020.74.6.809.

Kiani, Y. (2016), "Shear buckling of FG-CNT reinforced

composite plates using Chebyshev-Ritz method", *Compos. Part B: Eng.*, **105**, 176-187. https://doi.org/10.1016/J.COMPOSITESB.2016.09.001

Kolahdouzan, F., Gorbanpour Arani, A. and Abdollahian, M. (2018), "Buckling and free vibration analysis of FG-CNTRC-micro sandwich plate", *Steel Compos. Struct.*, **26**(3), 273-287. http://dx.doi.org/10.12989/scs.2018.26.3.273

Li, Q., Wu, D., Gao, W., Tin-Loi, F., Liu, Z. and Cheng, J. (2019), "Static bending and free vibration of organic solar cell resting on Winkler-Pasternak elastic foundation through the modified strain gradient theory", *Eur. J. Mech., A/Solids*, **78**, 103852. https://doi.org/10.1016/j.euromechsol.2019.103852

Li, Q., Wu, D., Gao, W. and Tin-Loi, F. (2020), "Size-dependent instability of organic solar cell resting on Winkler-Pasternak elastic foundation based on the modified strain gradient theory", *Int. J. Mech. Sci.*, **177**, 105306. https://doi.org/10.1016/j.ijmecsci.2019.105306

Lin, H.G., Cao, D.Q. and Xu, Y.Q. (2018), "Vibration, buckling and aeroelastic analyses of functionally graded multilayer graphene-nanoplatelets-reinforced composite plates embedded in piezoelectric layers", *Int. J. Appl. Mech.*, **10**(3), 1850023. https://doi.org/10.1142/S1758825118500230

Liu, H., Wu, H. and Lyu, Z. (2020), "Nonlinear resonance of FG multilayer beam-type nanocomposites: Effects of graphene nanoplatelet-reinforcement and geometric imperfection", *Aerosp. Sci. Technol.*, **98**, 105702. https://doi.org/10.1016/j.ast.2020.105702

Loghman, A. and Cheraghbak, A. (2018), "Agglomeration effects on electro-magneto-thermo elastic behavior of nano-composite piezoelectric cylinder", *Polym. Compos.*, **39**(5), 1594-1603. https://doi.org/10.1002/pc.24104

Mao, J.J. and Zhang, W. (2019), "Buckling and post-buckling analyses of functionally graded graphene reinforced piezoelectric plate subjected to electric potential and axial forces", *Compos. Struct.*, **216**, 392-405. https://doi.org/10.1016/j.compstruct.2019.02.095

Matouk, H., Bousahla, A.A., Heireche, H., Bourada, F., Bedia, E.A.A., Tounsi, A. and Benrahou, K.H. (2020), "Investigation on hygro-thermal vibration of P-FG and symmetric S-FG nanobeam using integral Timoshenko beam theory", *Adv. Nano Res.*, **8**(4), 293-305. https://doi.org/10.12989/anr.2020.8.4.293

Mehar, K., Panda, S.K., Bui, T.Q. and Mahapatra, T.R. (2017), "Nonlinear thermoelastic frequency analysis of functionally graded CNT-reinforced single/doubly curved shallow shell panels by FEM", *J. Thermal Stress.*, **40**(7), 899-916. https://doi.org/10.1080/01495739.2017.1318689

Mirjavadi, S.S., Forsat, M., Barati, M.R. and Hamouda, A.M.S. (2020a), "Investigating nonlinear forced vibration behavior of multi-phase nanocomposite annular sector plates using Jacobi elliptic functions", *Steel Compos. Struct.*, **36**(1), 87-101. https://doi.org/10.12989/scs.2020.36.1.087

Mirjavadi, S.S., Forsat, M., Barati, M.R., Hamouda, A., Mirjavadi, S.S., Forsat, M. and Hamouda, A. (2020b), "Nonlinear forced vibrations of multi-scale epoxy/CNT/fiberglass truncated conical shells and annular plates via 3D Mori-Tanaka scheme", *Steel Compos. Struct.*, **35**(6), 765-677. https://doi.org/10.12989/scs.2020.35.6.765

Mirjavadi, S.S., Nikookar, M., Mollaee, S., Forsat, M., Barati, M.R., Hamouda, A.M.S. and Hamouda, A.M.S. (2020c), "Analyzing exact nonlinear forced vibrations of two-phase magneto-electro-elastic nanobeams under an elliptic-type force", *Adv. Nano Res.*, **9**(1), 47-58. https://doi.org/10.12989/anr.2020.9.1.047

Mirsalehi, M., Azhari, M. and Amoushahi, H. (2017), "Buckling and free vibration of the FGM thin micro-plate based on the modified strain gradient theory and the spline finite strip method", *Eur. J. Mech., A/Solids*, **61**, 1-13. https://doi.org/10.1016/j.euromechsol.2016.08.008

Mirzaei, M. and Kiani, Y. (2016), "Free vibration of functionally graded carbon nanotube reinforced composite cylindrical panels", *Compos. Struct.*, **142**, 45-56. https://doi.org/10.1016/J.COMPSTRUCT.2015.12.071

Mohammadimehr, M., Arshid, E., Alhosseini, S.M.A.R., Amir, S. and Arani, M.R.G. (2019), "Free vibration analysis of thick cylindrical MEE composite shells reinforced CNTs with temperature-dependent properties resting on viscoelastic foundation", *Struct. Eng. Mech.*, **70**(6), 683-702. https://doi.org/10.12989/sem.2019.70.6.683

Mohammadzadeh-Keleshteri, M., Asadi, H. and Aghdam, M.M. (2017), "Geometrical nonlinear free vibration responses of FG-CNT reinforced composite annular sector plates integrated with piezoelectric layers", *Compos. Struct.*, **171**, 100-112. https://doi.org/10.1016/J.COMPSTRUCT.2017.01.048

Novoselov, K.S., Geim, A.K., Morozov, S.V., Jiang, D., Zhang, Y., Dubonos, S.V. and Firsov, A.A. (2004), "Electric field in atomically thin carbon films", *Science*, **306**(5696), 666-669. https://doi.org/10.1126/science.1102896

Paul, R., Kumbhakar, P. and Mitra, A.K. (2013), "A facile chemical synthesis of a novel photo catalyst: SWCNT/titania nanocomposite", *Adv. Nano Res.*, **1**(2), 71-82. https://doi.org/10.12989/anr.2013.1.2.071

Refrafi, S., Bousahla, A.A., Bouhadra, A., Menasria, A., Bourada, F., Tounsi, A. and Tounsi, A. (2020), "Effects of hygro-thermo-mechanical conditions on the buckling of FG sandwich plates resting on elastic foundations", *Comput. Concrete*, **25**(4), 311-325. https://doi.org/10.12989/cac.2020.25.4.311

Safaei, B. (2020), "The effect of embedding a porous core on the free vibration behavior of laminated composite plates", *Steel Compos. Struct.*, **35**(5), 659-670. http://dx.doi.org/10.12989/scs.2020.35.5.659

Safaei, B., Khoda, F.H. and Fattahi, A.M. (2019), "Non-classical plate model for single-layered graphene sheet for axial buckling", *Adv. Nano Res.*, **7**(4), 265-275. https://doi.org/10.12989/anr.2019.7.4.265

Safarpour, H., Esmailpoor Hajilak, Z. and Habibi, M. (2019), "A size-dependent exact theory for thermal buckling, free and forced vibration analysis of temperature dependent FG multilayer GPLRC composite nanostructures restring on elastic foundation", *Int. J. Mech. Mater. Des.*, **15**(3), 569-583. https://doi.org/10.1007/s10999-018-9431-8

Sahmani, S. and Aghdam, M.M. (2017a), "Axial postbuckling analysis of multilayer functionally graded composite nanoplates reinforced with GPLs based on nonlocal strain gradient theory", *Eur. Phys. J. Plus*, **132**(11), 1-17. https://doi.org/10.1140/epjp/i2017-11773-4

Sahmani, S. and Aghdam, M.M. (2017b), "Imperfection sensitivity of the size-dependent postbuckling response of pressurized FGM nanoshells in thermal environments", *Arch. Civil Mech. Eng.*, **17**(3), 623-638. https://doi.org/10.1016/j.acme.2017.01.004

Sahmani, S., Aghdam, M.M. and Bahrami, M. (2016), "Size-dependent axial buckling and postbuckling characteristics of cylindrical nanoshells in different temperatures", *Int. J. Mech. Sci.*, **107**, 170-179. https://doi.org/10.1016/j.ijmecsci.2016.01.014

Sahmani, S., Fattahi, A.M. and Ahmed, N.A. (2019), "Analytical mathematical solution for vibrational response of postbuckled laminated FG-GPLRC nonlocal strain gradient micro-/nanobeams", *Eng. Comput.*, **35**(4), 1173-1189. https://doi.org/10.1007/s00366-018-0657-8

Selim, B.A., Zhang, L.W. and Liew, K.M. (2016), "Vibration analysis of CNT reinforced functionally graded composite plates in a thermal environment based on Reddy's higher-order shear deformation theory", *Compos. Struct.*, **156**, 276-290.

https://doi.org/10.1016/j.compstruct.2015.10.026
Shen, H.-S., Xiang, Y., Lin, F. and Hui, D. (2017), "Buckling and postbuckling of functionally graded graphene-reinforced composite laminated plates in thermal environments", *Compos. Part B*: *Eng*., **119**, 67-78. https://doi.org/10.1016/J.COMPOSITESB.2017.03.020
Shingare, K.B. and Kundalwal, S.I. (2019), "Static and dynamic response of graphene nanocomposite plates with flexoelectric effect", *Mech. Mater*., **134**, 69-84. https://doi.org/10.1016/j.mechmat.2019.04.006
Sobhy, M. (2018), "Magneto-electro-thermal bending of FG-graphene reinforced polymer doubly-curved shallow shells with piezoelectromagnetic faces", *Compos. Struct*., **203**, 844-860. https://doi.org/10.1016/j.compstruct.2018.07.056
Talebizadehsardari, P., Eyvazian, A., Asmael, M., Karami, B., Shahsavari, D., and Mahani, R.B. (2020), "Static bending analysis of functionally graded polymer composite curved beams reinforced with carbon nanotubes", *Thin Wall. Struct*., **157**, 107139. https://doi.org/10.1016/j.tws.2020.107139
Thai, C.H., Ferreira, A.J.M. and Phung-Van, P. (2019), "Size dependent free vibration analysis of multilayer functionally graded GPLRC microplates based on modified strain gradient theory", *Compos. Part B*: *Eng*., **169**, 174-188. https://doi.org/10.1016/j.compositesb.2019.02.048
Van Thu, P. and Duc, N.D. (2016), "Nonlinear stability analysis of imperfect three-phase sandwich laminated polymer nanocomposite panels resting on elastic foundations in thermal environments", *VNU J. Sci.*: *Math. Phys*., **32**(1), 20-36. http://js.vnu.edu.vn/index.php/MaP/article/view/423
Yang, J., Chen, D. and Kitipornchai, S. (2018), "Buckling and free vibration analyses of functionally graded graphene reinforced porous nanocomposite plates based on Chebyshev-Ritz method", *Compos. Struct*., **193**, 281-294. https://doi.org/10.1016/J.COMPSTRUCT.2018.03.090
Yu, T., Hu, H., Zhang, J. and Bui, T.Q. (2019), "Isogeometric analysis of size-dependent effects for functionally graded microbeams by a non-classical quasi-3D theory", *Thin-Wall. Struct*., **138**, 1-14. https://doi.org/10.1016/j.tws.2018.12.006
Zenkour, A.M. (2016), "Buckling of a single-layered graphene sheet embedded in visco-Pasternak's medium via nonlocal first-order theory", *Adv. Nano Res*., **4**(4), 309-326. https://doi.org/10.12989/anr.2016.4.4.309
Zenkour, A.M. and Hafed, Z.S. (2020), "Bending response of functionally graded piezoelectric plates using a two variable shear deformation theory", *Adv. Aircr. Spacecr. Sci*., **7**(2), 115-134. https://doi.org/10.12989/aas.2020.7.2.115
Zhong, R., Wang, Q., Tang, J., Shuai, C. and Qin, B. (2018), "Vibration analysis of functionally graded carbon nanotube reinforced composites (FG-CNTRC) circular, annular and sector plates", *Compos. Struct*., **194**, 49-67. https://doi.org/10.1016/j.compstruct.2018.03.104
Zhu, P., Lei, Z.X. and Liew, K.M. (2012), "Static and free vibration analyses of carbon nanotube-reinforced composite plates using finite element method with first order shear deformation plate theory", *Compos. Struct*., **94**(4), 1450-1460. https://doi.org/10.1016/j.compstruct.2011.11.010

Appendix A

The used coefficients in Eq. (13) are introduced as follows

$$\begin{Bmatrix} N_{xx} \\ N_{yy} \\ M_{xxb} \\ M_{yyb} \\ M_{xxs} \\ M_{yys} \end{Bmatrix} = \int_z \left((Q_{11} \begin{bmatrix} 1 & -z & -\Phi(z) \\ z & -z^2 & -z\Phi(z) \\ \Phi(z) & -z\Phi(z) & -\Phi(z)^2 \end{bmatrix} + Q_{12} \begin{bmatrix} 1 & -z & -\Phi(z) \\ z & -z^2 & -z\Phi(z) \\ \Phi(z) & -z\Phi(z) & -\Phi(z)^2 \end{bmatrix} - E_z e_{31} \begin{bmatrix} 1 \\ z \\ \Phi(z) \end{bmatrix} \right) \left\{ \frac{\partial u}{\partial x}, \quad \frac{\partial^2 w_b}{\partial x^2}, \quad \frac{\partial^2 w_s}{\partial x^2}, \quad \frac{\partial v}{\partial y}, \quad \frac{\partial^2 w_b}{\partial y^2}, \quad \frac{\partial^2 w_s}{\partial y^2}, \quad \varphi \right\}^T dz, \tag{A1}$$

$$\begin{Bmatrix} N_{xy} \\ M_{xyb} \\ M_{xys} \end{Bmatrix} = \int_z Q_{66} \begin{bmatrix} 1 & -2z & -\Phi(z) & 1 \\ z & -2z^2 & -z\Phi(z) & z \\ \Phi(z) & -2z\Phi(z) & -\Phi(z)^2 & \Phi(z) \end{bmatrix} \left\{ \frac{\partial u}{\partial y}, \quad \frac{\partial^2 w_b}{\partial x \partial y}, \quad \frac{\partial^2 w_s}{\partial x \partial y}, \quad \frac{\partial v}{\partial x} \right\}^T dz, \tag{A2}$$

$$H_x = \int_z cos\left(\frac{\pi z}{h_f}\right) \left(-e_{15} \Phi'(z) \frac{\partial w_s}{\partial x} + e_{15} \frac{\partial w_s}{\partial x} + \kappa_{11} cos\left(\frac{\pi z}{h_f}\right) \frac{\partial \varphi}{\partial x} \right) dz, \tag{A3}$$

$$H_y = \int_z cos\left(\frac{\pi z}{h_f}\right) \left(-e_{24} \Phi'(z) \frac{\partial w_s}{\partial y} + e_{24} \frac{\partial w_s}{\partial y} + \kappa_{22} cos\left(\frac{\pi z}{h_f}\right) \frac{\partial \varphi}{\partial y} \right) dz, \tag{A4}$$

$$\begin{aligned} H_z = \int_z \frac{\pi}{h_f} sin\left(\frac{\pi z}{h_f}\right) \Bigg(& e_{31} \frac{\partial u}{\partial x} - z e_{31} \frac{\partial^2 w_b}{\partial x^2} - \Phi(z) e_{31} \frac{\partial^2 w_s}{\partial x^2} + e_{32} \frac{\partial v}{\partial y} \\ & - z e_{32} \frac{\partial^2 w_b}{\partial y^2} - \Phi(z) e_{32} \frac{\partial^2 w_s}{\partial y^2} - \frac{2}{h_f} \kappa_{33} \varphi_0 - \frac{2\pi}{h_f} sin(\frac{\pi z}{h_f})\ \kappa_{33} \varphi \Bigg) dz, \end{aligned} \tag{A5}$$

$$\begin{Bmatrix} Y_1 \\ Y_2 \end{Bmatrix} = \int_z G {l_0}^2 \begin{bmatrix} 2 & 1 + \Phi'(z) \\ 2\Phi'(z) & \Phi'(z)(1 + \Phi'(z)^2) \end{bmatrix} \begin{Bmatrix} \frac{\partial^2 w_b}{\partial x \partial y} \\ \frac{\partial^2 w_s}{\partial x \partial y} \end{Bmatrix} dz, \tag{A6}$$

$$\begin{Bmatrix} Y_3 \\ Y_4 \end{Bmatrix} = \int_z G {l_0}^2 \begin{bmatrix} 2 & -1 - \Phi'(z) \\ 2\Phi'(z) & -\Phi'(z)(1 + \Phi'(z)^2) \end{bmatrix} \begin{Bmatrix} \frac{\partial^2 w_b}{\partial x \partial y} \\ \frac{\partial^2 w_s}{\partial x \partial y} \end{Bmatrix} dz, \tag{A7}$$

$$\begin{Bmatrix} Y_5 \\ Y_6 \end{Bmatrix} = \int_z G {l_0}^2 \begin{bmatrix} 1 & \frac{1}{2}(1 + \Phi'(z)) & -1 & -\frac{1}{2}(1 + \Phi'(z)) \\ \Phi'(z) & \frac{1}{2}(1 + \Phi'(z)) & -\Phi'(z) & -\frac{1}{2}(1 + \Phi'(z)) \end{bmatrix} \left\{ \frac{\partial^2 w_b}{\partial y^2}, \quad \frac{\partial^2 w_s}{\partial y^2}, \quad \frac{\partial^2 w_b}{\partial x^2}, \quad \frac{\partial^2 w_s}{\partial x^2} \right\}^T dz, \tag{A8}$$

$$\begin{Bmatrix} Y_7 \\ Y_8 \end{Bmatrix} = \int_z \frac{1}{2} G {l_0}^2 \begin{bmatrix} \Phi''(z)^2 & \Phi''(z) & -\Phi''(z) \\ \Phi''(z) & 1 & -1 \end{bmatrix} \left\{ \frac{\partial w_s}{\partial y}, \quad \frac{\partial^2 v}{\partial x^2}, \quad \frac{\partial^2 u}{\partial x \partial y} \right\}^T dz, \tag{A9}$$

$$\begin{Bmatrix} Y_9 \\ Y_{10} \end{Bmatrix} = \int_z \frac{1}{2} G {l_0}^2 \begin{bmatrix} -\Phi''(z)^2 & \Phi''(z) & -\Phi''(z) \\ -\Phi''(z) & 1 & -1 \end{bmatrix} \left\{ \frac{\partial w_s}{\partial x}, \quad \frac{\partial^2 v}{\partial x \partial y}, \quad \frac{\partial^2 u}{\partial y^2} \right\}^T dz, \tag{A10}$$

$$\begin{Bmatrix} X_1 \\ X_2 \\ X_3 \end{Bmatrix} = \int_z 2G {l_1}^2 \begin{bmatrix} 1 & -z & -\Phi(z) & 1 & -z & -\Phi(z) \\ z & -z^2 & -z\Phi(z) & z & -z^2 & -z\Phi(z) \\ \Phi(z) & -z\Phi(z) & -\Phi(z)^2 & \Phi(z) & -z\Phi(z) & -\Phi(z)^2 \end{bmatrix} \left\{ \frac{\partial^2 u}{\partial x^2}, \quad \frac{\partial^3 w_b}{\partial x^3}, \quad \frac{\partial^3 w_s}{\partial x^3}, \quad \frac{\partial^2 v}{\partial x \partial y}, \quad \frac{\partial^3 w_b}{\partial x \partial y^2}, \quad \frac{\partial^3 w_s}{\partial x \partial y^2} \right\}^T dz, \tag{A11}$$

$$\begin{Bmatrix} X_4 \\ X_5 \\ X_6 \end{Bmatrix} = \int_z 2G{l_1}^2 \begin{bmatrix} 1 & -z & -\Phi(z) & 1 & -z & -\Phi(z) \\ z & -z^2 & -z\Phi(z) & z & -z^2 & -z\Phi(z) \\ \Phi(z) & -z\Phi(z) & -\Phi(z)^2 & \Phi(z) & -z\Phi(z) & -\Phi(z)^2 \end{bmatrix} \left\{ \frac{\partial^2 u}{\partial x \partial y}, \frac{\partial^3 w_b}{\partial x^2 \partial y}, \frac{\partial^3 w_s}{\partial x^2 \partial y}, \frac{\partial^2 v}{\partial y^2}, \frac{\partial^3 w_b}{\partial y^3}, \frac{\partial^3 w_s}{\partial y^3} \right\}^T dz, \tag{A12}$$

$$\begin{Bmatrix} X_7 \\ X_8 \end{Bmatrix} = \int_z -2G{l_1}^2 \begin{bmatrix} 1 & \Phi'(z) & 1 & \Phi'(z) \\ \Phi'(z) & \Phi'(z)^2 & \Phi'(z) & \Phi'(z)^2 \end{bmatrix} \left\{ \frac{\partial^2 w_b}{\partial x^2}, \frac{\partial^2 w_s}{\partial x^2}, \frac{\partial^2 w_b}{\partial y^2}, \frac{\partial^2 w_s}{\partial y^2} \right\}^T dz, \tag{A13}$$

$$\begin{Bmatrix} T_1 \\ T_2 \\ T_3 \\ T_4 \end{Bmatrix} = \int_z \frac{4}{5}{l_2}^2 G \begin{bmatrix} 1 & -z & -\Phi(z) & -1 & z & -\Phi(z) & -1 & \frac{1}{2}\Phi''(z) \\ z & -z^2 & -z\Phi(z) & -z & z^2 & -z\Phi(z) & -z & \frac{1}{2}z\Phi''(z) \\ \Phi(z) & -z\Phi(z) & -z\Phi(z)^2 & -\Phi(z) & z\Phi(z) & -\Phi(z)^2 & -\Phi(z) & \frac{1}{2}\Phi(z)\Phi''(z) \\ \Phi''(z) & -z\Phi''(z) & -\Phi''(z)\Phi(z) & -\Phi''(z) & z\Phi''(z) & -\Phi(z)\Phi''(z) & -\Phi''(z) & \frac{1}{2}\Phi''(z)^2 \end{bmatrix} \left\{ \frac{\partial^2 u}{\partial x^2}, \frac{\partial^3 w_b}{\partial x^3}, \frac{\partial^3 w_s}{\partial x^3}, \frac{\partial^2 v}{\partial x \partial y}, \frac{\partial^3 w_b}{\partial x \partial y^2}, \frac{\partial^3 w_s}{\partial x \partial y^2}, \frac{\partial^2 u}{\partial y^2}, \frac{\partial w_s}{\partial x} \right\}^T dz, \tag{A14}$$

$$\begin{Bmatrix} T_5 \\ T_6 \\ T_7 \\ T_8 \end{Bmatrix} = \int_z \frac{4}{5}{l_2}^2 G \begin{bmatrix} 1 & -z & -\Phi(z) & -1 & z & \Phi(z) & -1 & \frac{1}{2}\Phi''(z) \\ z & -z^2 & -z\Phi(z) & -z & z^2 & z\Phi(z) & -z & \frac{1}{2}z\Phi''(z) \\ \Phi(z) & -z\Phi(z) & -z\Phi(z)^2 & -\Phi(z) & z\Phi(z) & \Phi(z)^2 & -\Phi(z) & \frac{1}{2}\Phi(z)\Phi''(z) \\ \Phi''(z) & -z\Phi''(z) & -\Phi''(z)\Phi(z) & -\Phi''(z) & z\Phi''(z) & \Phi(z)\Phi''(z) & -\Phi''(z) & \frac{1}{2}\Phi''(z)^2 \end{bmatrix} \left\{ \frac{\partial^2 v}{\partial y^2}, \frac{\partial^3 w_b}{\partial y^3}, \frac{\partial^3 w_s}{\partial y^3}, \frac{\partial^2 u}{\partial x \partial y}, \frac{\partial^3 w_b}{\partial x \partial y^2}, \frac{\partial^3 w_s}{\partial x \partial y^2}, \frac{\partial^2 v}{\partial x^2}, \frac{\partial w_s}{\partial y} \right\}^T dz, \tag{A15}$$

$$\begin{Bmatrix} T_9 \\ T_{10} \end{Bmatrix} = \int_z \frac{2}{5} G{l_2}^2 \begin{bmatrix} 1 & 2\Phi'(z) - 1 & 1 & \Phi'(z) \\ \Phi'(z) & 2\Phi'(z)^2 - 1 & \Phi'(z) & \Phi'(z)^2 \end{bmatrix} \left\{ \frac{\partial^2 w_b}{\partial x^2}, \frac{\partial^2 w_s}{\partial x^2}, \frac{\partial^2 w_b}{\partial y^2}, \frac{\partial^2 w_s}{\partial y^2} \right\}^T dz, \tag{A16}$$

$$\begin{Bmatrix} T_{11} \\ T_{12} \\ T_{13} \\ T_{14} \end{Bmatrix} = \int_z \frac{2}{5}{l_2}^2 G \begin{bmatrix} -1 & z & -\Phi(z) & \frac{8}{3} & -4z & 4\Phi(z) & \frac{4}{3} & -\frac{1}{3}\Phi''(z) \\ -z & z^2 & -z\Phi(z) & \frac{8}{3}z & -4z^2 & 4z\Phi(z) & \frac{4}{3}z & -\frac{1}{3}z\Phi''(z) \\ -\Phi(z) & z\Phi(z) & -z\Phi(z)^2 & \frac{8}{3}\Phi(z) & -4z\Phi(z) & 4\Phi(z)^2 & \frac{4}{3}\Phi(z) & -\frac{1}{3}\Phi(z)\Phi''(z) \\ -\Phi''(z) & z\Phi''(z) & -\Phi''(z)\Phi(z) & \frac{8}{3}\Phi''(z) & -4z\Phi''(z) & 4\Phi(z)\Phi''(z) & \frac{4}{3}\Phi''(z) & -\frac{1}{3}\Phi''(z)^2 \end{bmatrix} \left\{ \frac{\partial^2 u}{\partial x^2}, \frac{\partial^3 w_b}{\partial x^3}, \frac{\partial^3 w_s}{\partial x^3}, \frac{\partial^2 v}{\partial x \partial y}, \frac{\partial^3 w_b}{\partial y^2 \partial x}, \frac{\partial^2 u}{\partial x^2}, \frac{\partial^3 w_s}{\partial y^2 \partial x}, \frac{\partial w_s}{\partial x} \right\}^T dz, \tag{A17}$$

$$\begin{Bmatrix} T_{15} \\ T_{16} \\ T_{17} \\ T_{18} \end{Bmatrix} = \int_z \frac{2}{5}{l_2}^2 G \begin{bmatrix} -1 & z & \Phi(z) & \frac{8}{3} & -4z & 4\Phi(z) & \frac{4}{3} & -\frac{1}{3}\Phi''(z) \\ -z & z^2 & z\Phi(z) & \frac{8}{3}z & -4z^2 & 4z\Phi(z) & \frac{4}{3}z & -\frac{1}{3}z\Phi''(z) \\ -\Phi(z) & z\Phi(z) & z\Phi(z)^2 & \frac{8}{3}\Phi(z) & -4z\Phi(z) & 4\Phi(z)^2 & \frac{4}{3}\Phi(z) & -\frac{1}{3}\Phi(z)\Phi''(z) \\ -\Phi''(z) & z\Phi''(z) & \Phi''(z)\Phi(z) & \frac{8}{3}\Phi''(z) & -4z\Phi''(z) & 4\Phi(z)\Phi''(z) & \frac{4}{3}\Phi''(z) & -\frac{1}{3}\Phi''(z)^2 \end{bmatrix} \left\{ \frac{\partial^2 v}{\partial y^2}, \frac{\partial^3 w_b}{\partial y^3}, \frac{\partial^3 w_s}{\partial y^3}, \frac{\partial^2 u}{\partial x \partial y}, \frac{\partial^3 w_b}{\partial x^2 \partial y}, \frac{\partial^3 w_s}{\partial x^2 \partial y}, \frac{\partial^2 v}{\partial x^2}, \frac{\partial w_s}{\partial x} \right\}^T dz, \tag{A18}$$

$$\begin{Bmatrix} T_{19} \\ T_{20} \\ T_{21} \\ T_{22} \end{Bmatrix} = \int_z \frac{2}{5} {l_2}^2 G \begin{bmatrix} -1 & z & \Phi(z) & \frac{2}{3} & -z & \Phi(z) & -\frac{1}{3} & -\frac{4}{3}\Phi''(z) \\ -z & z^2 & z\Phi(z) & \frac{2}{3}z & -z^2 & z\Phi(z) & -\frac{1}{3}z & -\frac{4}{3}z\Phi''(z) \\ -\Phi(z) & z\Phi(z) & z\Phi(z)^2 & \frac{2}{3}\Phi(z) & -z\Phi(z) & \Phi(z)^2 & -\frac{1}{3}\Phi(z) & -\frac{4}{3}f(z)\Phi''(z) \\ -\Phi''(z) & z\Phi''(z) & \Phi''(z)\Phi(z) & \frac{2}{3}\Phi''(z) & -z\Phi''(z) & \Phi(z)\Phi''(z) & -\frac{1}{3}\Phi''(z) & -\frac{4}{3}\Phi''(z)^2 \end{bmatrix} \left\{ \frac{\partial^2 u}{\partial x^2}, \frac{\partial^3 w_b}{\partial x^3}, \frac{\partial^3 w_s}{\partial x^3}, \frac{\partial^2 v}{\partial x \partial y}, \frac{\partial^3 w_b}{\partial y^2 \partial x}, \frac{\partial^3 w_s}{\partial y^2 \partial x}, \frac{\partial^2 u}{\partial y^2}, \frac{\partial w_s}{\partial x} \right\}^T dz, \tag{A19}$$

$$\begin{Bmatrix} T_{23} \\ T_{24} \\ T_{25} \\ T_{26} \end{Bmatrix} = \int_z \frac{2}{5} {l_2}^2 G \begin{bmatrix} -1 & z & \Phi(z) & -\frac{2}{3} & z & \Phi(z) & -\frac{1}{3} & -\frac{4}{3}\Phi''(z) \\ -z & z^2 & z\Phi(z) & -\frac{2}{3}z & z^2 & z\Phi(z) & -\frac{1}{3}z & -\frac{4}{3}z\Phi''(z) \\ -\Phi(z) & z\Phi(z) & z\Phi(z)^2 & -\frac{2}{3}\Phi(z) & z\Phi(z) & \Phi(z)^2 & -\frac{1}{3}\Phi(z) & -\frac{4}{3}\Phi(z)\Phi''(z) \\ -\Phi''(z) & z\Phi''(z) & \Phi''(z)\Phi(z) & -\frac{2}{3}\Phi''(z) & z\Phi''(z) & \Phi(z)\Phi''(z) & -\frac{1}{3}\Phi''(z) & -\frac{4}{3}\Phi''(z)^2 \end{bmatrix} \left\{ \frac{\partial^2 v}{\partial y^2}, \frac{\partial^3 w_b}{\partial y^3}, \frac{\partial^3 w_s}{\partial y^3}, \frac{\partial^2 u}{\partial x \partial y}, \frac{\partial^3 w_b}{\partial x^2 \partial y}, \frac{\partial^3 w_s}{\partial x^2 \partial y}, \frac{\partial^2 v}{\partial x^2}, \frac{\partial w_s}{\partial y} \right\}^T dz, \tag{A20}$$

$$\begin{Bmatrix} T_{27} \\ T_{28} \end{Bmatrix} = \int_z \frac{2}{15} G {l_2}^2 \begin{bmatrix} -4 & -8\Phi'(z) + 4 & 1 & 2\Phi'(z) - 1 \\ -4\Phi'(z) & -8\Phi'(z)^2 + 4\Phi'(z) & \Phi'(z) & 2\Phi'(z)^2 - \Phi'(z) \end{bmatrix} \left\{ \frac{\partial^2 w_b}{\partial x^2}, \frac{\partial^2 w_s}{\partial x^2}, \frac{\partial^2 w_b}{\partial y^2}, \frac{\partial^2 w_s}{\partial y^2} \right\}^T dz, \tag{A21}$$

$$\begin{Bmatrix} T_{29} \\ T_{30} \end{Bmatrix} = \int_z \frac{2}{15} G {l_2}^2 \begin{bmatrix} -1 & -2\Phi'(z) + 1 & 4 & 8\Phi'(z) + 4 \\ -\Phi'(z) & -2\Phi'(z)^2 + \Phi'(z) & 4\Phi'(z) & 8\Phi'(z)^2 + 4\Phi'(z) \end{bmatrix} \left\{ \frac{\partial^2 w_b}{\partial x^2}, \frac{\partial^2 w_s}{\partial x^2}, \frac{\partial^2 w_b}{\partial y^2}, \frac{\partial^2 w_s}{\partial y^2} \right\}^T dz, \tag{A22}$$

$$\begin{Bmatrix} T_{31} \\ T_{32} \end{Bmatrix} = \int_z \frac{2}{3} G {l_2}^2 \begin{bmatrix} -2\Phi'(z) + \Phi'(z) & -1 \\ -2\Phi'(z)^2 + \Phi'(z)^2 & -\Phi'(z) \end{bmatrix} \begin{Bmatrix} \frac{\partial^2 w_s}{\partial y \partial x} \\ \frac{\partial^2 w_b}{\partial y \partial x} \end{Bmatrix} dz \tag{A23}$$

$$\begin{aligned} I_0, I_1, I_2, I_3, I_4, I_5 = & \int_{\frac{h_c}{2}}^{\frac{h_c}{2}+h_t} \rho_f(1, z, z^2, \Phi(z), z\Phi(z), \Phi(z)^2) dz + \int_{-\frac{h_c}{2}}^{\frac{h_c}{2}} \rho_c(z)(1, z, z^2, \Phi(z), z\Phi(z), \Phi(z)^2) dz \\ & + \int_{-\frac{h_c}{2}-h_b}^{-\frac{h_c}{2}} \rho_f(1, z, z^2, \Phi(z), z\Phi(z), \Phi(z)^2) dz, \end{aligned} \tag{A24}$$

Appendix B

The non-zero arrays of stiffness, damping, and mass matrices of Eq. (45a) are defined as

$$K_{11} = \frac{1}{2}T_0\alpha^2\beta^2 + 2K_0\alpha^2\beta^2 + \frac{14}{15}G_0\alpha^2\beta^2 + 2K_0\alpha^4 + \frac{4}{5}G_0\alpha^4 + Q_{110}\alpha^2 + Q_{660}\beta^2 + \frac{1}{2}T_0\beta^4 + \frac{2}{5}G_0\beta^4,$$

$$K_{12} = -\frac{1}{2}T_0\alpha^3\beta + 2K_0\alpha^3\beta + 2K_0\alpha\beta^3 + \frac{4}{15}G_0\alpha^3\beta + Q_{120}\alpha\beta + Q_{660}\alpha\beta - \frac{1}{2}T_0\alpha\beta^3,$$

$$K_{13} = -4K_1\alpha^3\beta^2 - 2K_1\alpha\beta^4 - \frac{6}{5}G_1\alpha^3\beta^2 - Q_{121}\alpha\beta^2 - 2Q_{661}\alpha\beta^2 - \frac{2}{5}G_1\alpha\beta^4 - 2K_1\alpha^5 - \frac{4}{5}G_1\alpha^5 - Q_{111}\alpha^3,$$

$$K_{14} = -4K_3\alpha^3\beta^2 - 2K_3\alpha\beta^4 - \frac{6}{5}G_3\alpha^3\beta^2 - Q_{123}\alpha\beta^2 - 2Q_{663}\alpha\beta^2 - \frac{2}{5}G_3\alpha\beta^4 - 2K_3\alpha^5 - \frac{4}{5}G_3\alpha^5 - Q_{113}\alpha^3,$$

$$K_{15} = -Q_{136}\alpha,$$

$$K_{21} = 2K_0\alpha\beta^3 + 2K_0\alpha^3\beta + \frac{4}{15}G_0\alpha^3\beta + \frac{4}{15}G_0\alpha\beta^3 + Q_{120}\alpha\beta + Q_{660}\alpha\beta - \frac{1}{2}T_0\alpha^3\beta - \frac{1}{2}T_0\alpha\beta^3,$$

$$K_{22} = 2K_0\alpha^2\beta^2 + \frac{4}{3}G_0\alpha^2\beta^2 + \frac{1}{2}T_0\alpha^2\beta^2 + Q_{220}\beta^2 + Q_{660}\alpha^2 + \frac{1}{2}T_0\alpha^4 + 2K_0\beta^4 + \frac{8}{15}G_0\alpha^4 + \frac{4}{5}G_0\beta^4,$$

$$K_{23} = -4K_1\alpha^2\beta^3 - 2K_1\alpha^4\beta - \frac{8}{5}G_1\alpha^2\beta^3 - \frac{4}{5}G_1\alpha^4\beta - Q_{121}\alpha^2\beta - 2Q_{661}\alpha^2\beta - Q_{221}\beta^3 - 2K_1\beta^5 - \frac{4}{5}G_1\beta^5,$$

$$K_{24} = -4K_3\alpha^2\beta^3 - 2K_3\alpha^4\beta - \frac{8}{5}G_3\alpha^2\beta^3 - \frac{4}{5}G_3\alpha^4\beta - Q_{123}\alpha^2\beta - 2Q_{663}\alpha^2\beta - Q_{223}\beta^3 - 2K_3\beta^5 - \frac{4}{5}G_3\beta^5,$$

$$K_{25} = -Q_{236}\beta$$

$$K_{31} = 4K_1\alpha^3\beta^2 + 2K_1\alpha\beta^4 - 2Q_{661}\alpha\beta^2 + \frac{4}{5}G_1\alpha\beta^4 - Q_{121}\alpha\beta^2 + \frac{8}{5}G_1\alpha^3\beta^2 - Q_{111}\alpha^3 + \frac{4}{5}G_1\alpha^5 + 2K_1\alpha^5,$$

$$K_{32} = 2K_1\alpha^4\beta + 4K_1\alpha^2\beta^3 - 2Q_{661}\alpha^2\beta + \frac{8}{5}G_1\alpha^2\beta^3 - Q_{121}\alpha^2\beta + \frac{4}{5}G_1\alpha^4\beta - Q_{221}\beta^3 + 2K_1\beta^5 + \frac{4}{5}G_1\beta^5,$$

$$\begin{aligned} K_{33} = {} & -2K_2\alpha^2\beta^4 - 4K_2\alpha^4\beta^2 - 4K_2\alpha^2\beta^4 + 4K_0\alpha^2\beta^2 + \frac{88}{75}G_0\alpha^2\beta^2 + 4Q_{662}\alpha^2\beta^2 - \frac{12}{5}G_2\alpha^2\beta^4 \\ & -2K_2\alpha^4\beta^2 + 2Q_{122}\alpha^2\beta^2 - \frac{12}{5}G_2\alpha^4\beta^2 + Q_{112}\alpha^4 + Q_{222}\beta^4 - \frac{4}{5}G_2\alpha^6 + \frac{8}{75}G_0\beta^4 \\ & -2K_2\alpha^6 - 2K_2\beta^6 + 2K_0\beta^4 + \frac{8}{15}G_0\alpha^4 - \frac{4}{5}G_2\beta^6 + 2T_0\beta^4 + 2T_0\alpha^4 + 2K_0\alpha^4, \end{aligned}$$

$$\begin{aligned} K_{34} = {} & Q_{224}\beta^4 + T_1\beta^4 + T_1\alpha^4 + Q_{114}\alpha^4 - 2K_4\alpha^6 + 2K_6\beta^4 + \frac{8}{15}G_6\alpha^4 + \frac{8}{75}G_6\beta^4 + 2K_6\alpha^4 \\ & -2K_4\beta^6 - \frac{4}{5}G_4\alpha^6 - \frac{4}{5}G_4\beta^6 - 6K_4\alpha^2\beta^4 + 4Q_{664}\alpha^2\beta^2 - 6K_4\alpha^4\beta^2 + 4K_6\alpha^2\beta^2 + \frac{88}{75}G_6\alpha^2\beta^2 \\ & -\frac{12}{5}G_4\alpha^2\beta^4 + 2Q_{124}\alpha^2\beta^2 - \frac{12}{5}G_4\alpha^4\beta^2 + T_0\alpha^4 + T_0\beta^4, \end{aligned}$$

$$K_{35} = Q_{137}\alpha^2 + Q_{237}\beta^2,$$

$$K_{41} = 2K_3\alpha^5 - Q_{113}\alpha^3 + \frac{4}{5}G_3\alpha^5 + 2K_3\alpha\beta^4 + \frac{8}{5}G_3\alpha^3\beta^2 - Q_{123}\alpha\beta^2 + 4K_3\alpha^3\beta^2 - 2Q_{663}\alpha\beta^2 + \frac{4}{5}G_3\alpha\beta^4,$$

$$K_{42} = 2K_3\beta^5 - Q_{223}\beta^3 + \frac{4}{5}G_3\beta^5 + 2K_3\alpha^4\beta - Q_{123}\alpha^2\beta + \frac{4}{5}G_3\alpha^4\beta + 4K_3\alpha^2\beta^3 - 2Q_{663}\alpha^2\beta + \frac{8}{5}G_3\alpha^2\beta^3,$$

$$K_{43} = Q_{224}\beta^4 + T_1\beta^4 + T_1\alpha^4 + Q_{114}\alpha^4 - 2K_4\alpha^6 + 2K_6\beta^4 + \frac{8}{15}G_6\alpha^4 + \frac{8}{75}G_6\beta^4 + 2K_6\alpha^4 - 2K_4\beta^6 - \frac{4}{5}G_4\alpha^6 - \frac{4}{5}G_4\beta^6 - 6K_4\alpha^2\beta^4 + 4Q_{664}\alpha^2\beta^2 - 6K_4\alpha^4\beta^2 + 4K_6\alpha^2\beta^2 - \frac{4}{25}G_6\alpha^2\beta^2 - \frac{12}{5}G_4\alpha^2\beta^4 + 2Q_{124}\alpha^2\beta^2 - \frac{12}{5}G_4\alpha^4\beta^2 + T_0\alpha^4 + T_0\beta^4,$$

$$K_{44} = -\frac{12}{5}G_5\alpha^4\beta^2 - 6K_5\alpha^2\beta^4 + 2Q_{125}\alpha^2\beta^2 - 6K_5\alpha^4\beta^2 + 4Q_{665}\alpha^2\beta^2 - \frac{12}{5}G_5\alpha^2\beta^4 + 4K_7\alpha^2\beta^2 + \frac{88}{75}G_7\alpha^2\beta^2 + Q_{225}\beta^4 + Q_{552}\alpha^2 + Q_{115}\alpha^4 + \frac{1}{2}T_2\beta^4 - 2K_5\beta^6 + \frac{1}{2}T_4\beta^2 - \frac{4}{5}G_5\beta^6 + 2K_7\alpha^4 - \frac{4}{5}G_5\alpha^6 + 2K_7\beta^4 - 2K_5\alpha^6 + \frac{1}{2}T_4\alpha^2 + \frac{8}{75}G_7\beta^4 + \frac{1}{2}T_2\alpha^4 + \frac{8}{15}G_7\alpha^4 + T_1\beta^4 + T_1\alpha^4 + \frac{1}{2}T_0\alpha^4 + \frac{1}{2}T_0\beta^4,$$

$$K_{45} = Q_{138}\alpha^2 + Q_{238}\beta^2,$$

$$K_{51} = -Q_{136}\alpha,$$

$$K_{52} = -Q_{236}\beta,$$

$$K_{53} = Q_{137}\alpha^2 + Q_{237}\beta^2,$$

$$K_{54} = Q_{138}\alpha^2 + Q_{238}\beta^2,$$

$$K_{55} = -R_{111}\alpha^2 - R_{221}\beta^2 - R_{331},$$

$$m_{11} = I_0, \quad m_{13} = -I_1\alpha, \quad m_{14} = -I_3\alpha, \quad m_{22} = I_0,$$

$$m_{23} = -I_1\beta, \quad m_{24} = -I_3\beta, \quad m_{31} = -I_1\alpha, \quad m_{32} = -I_1\beta,$$

$$m_{33} = I_2\alpha^2 - I_2\beta^2 + I_0, \quad m_{34} = I_4\alpha^2 - I_4\beta^2 + I_0, \quad m_{55} = I_6, \quad m_{41} = -I_3\alpha,$$

$$m_{42} = -I_3\beta, \quad m_{43} = I_4\alpha^2 - I_4\beta^2 + I_0, \quad m_{44} = I_0,$$

$$C_{33} = C_{34} = C_{43} = C_{44} = D$$

in which

$$Q_{110}, Q_{111}, Q_{112}, Q_{113}, Q_{114}, Q_{115} = \int_{\frac{h_c}{2}}^{\frac{h_c}{2}+h_t} Q_{11}(z)(1, z, z^2, \Phi(z), z\Phi(z), \Phi(z)^2)dz + \int_{-\frac{h_c}{2}}^{\frac{h_c}{2}} Q_{11c}(z)(1, z, z^2, \Phi(z), z\Phi(z), \Phi(z)^2)dz + \int_{-\frac{h_c}{2}-h_b}^{-\frac{h_c}{2}} Q_{11}(z)(1, z, z^2, \Phi(z), z\Phi(z), \Phi(z)^2)dz$$

$$Q_{120}, Q_{121}, Q_{122}, Q_{123}, Q_{124}, Q_{125} = \int_{\frac{h_c}{2}}^{\frac{h_c}{2}+h_t} Q_{12}(z)(1, z, z^2, \Phi(z), z\Phi(z), \Phi(z)^2)dz + \int_{-\frac{h_c}{2}}^{\frac{h_c}{2}} Q_{12c}(z)(1, z, z^2, \Phi(z), z\Phi(z), \Phi(z)^2)dz + \int_{-\frac{h_c}{2}-h_b}^{-\frac{h_c}{2}} Q_{12}(z)(1, z, z^2, \Phi(z), z\Phi(z), \Phi(z)^2)dz$$

$$Q_{220}, Q_{221}, Q_{222}, Q_{223}, Q_{224}, Q_{225} = \int_{\frac{h_c}{2}}^{\frac{h_c}{2}+h_t} Q_{22}(z)(1, z, z^2, \Phi(z), z\Phi(z), \Phi(z)^2)dz + \int_{-\frac{h_c}{2}}^{\frac{h_c}{2}} Q_{22c}(z)(1, z, z^2, \Phi(z), z\Phi(z), \Phi(z)^2)dz + \int_{-\frac{h_c}{2}-h_b}^{-\frac{h_c}{2}} Q_{22}(z)(1, z, z^2, \Phi(z), z\Phi(z), \Phi(z)^2)dz$$

$$Q_{136}, Q_{137}, Q_{138} = \int_{\frac{h_c}{2}}^{\frac{h_c}{2}+h_t} e_{13}\left(\frac{\pi}{h_t} sin(\frac{\pi z}{h_t})\right)(1, z, \Phi(z))dz + \int_{-\frac{h_c}{2}-h_b}^{-\frac{h_c}{2}} e_{13}\left(\frac{\pi}{h_t} sin\left(\frac{\pi z}{h_t}\right)\right)(1, z, \Phi(z))dz$$

$$Q_{236}, Q_{237}, Q_{238} = \int_{\frac{h_c}{2}}^{\frac{h_c}{2}+h_t} e_{23}\left(\frac{\pi}{h_t} sin\left(\frac{\pi z}{h_t}\right)\right)(1, z, \Phi(z))dz + \int_{-\frac{h_c}{2}-h_b}^{-\frac{h_c}{2}} e_{23}\left(\frac{\pi}{h_t} sin\left(\frac{\pi z}{h_t}\right)\right)(1, z, \Phi(z))dz$$

$$R_{111}, R_{221} = \int_{\frac{h_c}{2}}^{\frac{h_c}{2}+h_t} (\kappa_{11}, \kappa_{22})\left(cos\left(\frac{\pi z}{h_t}\right)\right)^2 dz + \int_{-\frac{h_c}{2}-h_b}^{-\frac{h_c}{2}} (\kappa_{11}, \kappa_{22})\left(cos\left(\frac{\pi z}{h_b}\right)\right)^2 dz$$

$$R_{333} = \int_{\frac{h_c}{2}}^{\frac{h_c}{2}+h_t} (\kappa_{33})\left(\frac{\pi}{{h_t}^2} sin\left(\frac{\pi z}{h_t}\right)\right)\left(\pi^2 sin\left(\frac{\pi z}{h_t}\right)\right) dz + \int_{-\frac{h_c}{2}-h_b}^{-\frac{h_c}{2}} (\kappa_{33})\left(\frac{\pi}{{h_b}^2} sin\left(\frac{\pi z}{h_b}\right)\right)\left(\pi^2 sin\left(\frac{\pi z}{h_b}\right)\right) dz$$

$$T_0, T_1, T_2, T_3, T_4, T_5 = \int_i^j {L_0}^2 G(1, \Phi'(z), \Phi'(z)^2, \Phi''(z), \Phi''(z)^2)dz + \int_{-\frac{h_c}{2}}^{\frac{h_c}{2}} {L_0}^2 G(1, \Phi'(z), \Phi'(z)^2, \Phi''(z), \Phi''(z)^2)dz$$

$$K_0, K_1, K_2, K_3, K_4, K_5, K_6, K_7 = \int_i^j {L_1}^2 G(1, z, z^2, \Phi(z), z\Phi(z), \Phi(z)^2, \Phi'(z), \Phi'(z)^2)dz + \int_{-\frac{h_c}{2}}^{\frac{h_c}{2}} {L_1}^2 G(1, z, z^2, \Phi(z), z\Phi(z), \Phi(z)^2, \Phi'(z), \Phi'(z)^2)dz$$

$$G_0, G_1, G_2, G_3, G_4, G_5, G_6, G_7, G_8 = \int_i^j {L_2}^2 G(1, z, z^2, \Phi(z), z\Phi(z), \Phi(z)^2, \Phi'(z), \Phi'(z)^2)dz + \int_{-\frac{h_c}{2}}^{\frac{h_c}{2}} {L_2}^2 G(1, z, z^2, \Phi(z), z\Phi(z), \Phi(z)^2, \Phi'(z), \Phi'(z)^2)dz$$

$$i = -\frac{h_c}{2}, -\frac{h_c}{2} - h_b j = \frac{h_c}{2} + h_t, \frac{h_c}{2}$$